

Asparaginyl and Aspartyl Hydroxylation of the Cytoskeletal Ankyrin Family Is Catalysed by Factor Inhibiting Hypoxia-Inducible Factor (FIH)

Ming Yang[†], Wei Ge^{†1}, Rasheduzzaman Chowdhury^{†1}, Timothy D. W. Claridge^{†1}, Holger B. Kramer[‡], Bernhard Schmierer[§], Michael A. McDonough[†], Lingzhi Gong[†], Benedikt M. Kessler[‡], Peter J. Ratcliffe[‡], Mathew L. Coleman^{‡2} and Christopher J. Schofield^{†2}

From [†]Chemistry Research Laboratory and Oxford Centre for Integrative Systems Biology, University of Oxford, Oxford OX1 3TA, United Kingdom, [§]the Department of Biochemistry and Oxford Centre for Integrative Systems Biology, University of Oxford, South Parks Road, Oxford OX1 3QU and [‡]Henry Wellcome Building for Molecular Physiology, University of Oxford, Oxford OX3 7BN, United Kingdom

Running title: Ankyrin asparaginyl and aspartyl hydroxylation by FIH

Address correspondence to: Christopher J. Schofield, Chemistry Research Laboratory, University of Oxford, 12 Mansfield Road, Oxford OX1 3TA, United Kingdom. Phone: 44-1865-275625; Fax: 44-1865-275674; E-mail: christopher.schofield@chem.ox.ac.uk

SUPPLEMENTAL DATA

Figure S1 Peptide fragments derived from the human ankyrinR ARD are FIH substrates. Peptides corresponding to (A) AnkyrinR₉₂₋₁₀₉ (EVVRELVNYGANVNAQSQ) (B) AnkyrinR₁₂₅₋₁₄₂ (EVVKFLENGANQNVATE) (C) AnkyrinR₂₂₀₋₂₃₇ (NVAQLLLNRGSSVNFTPQ) (D) AnkyrinR₄₅₁₋₄₆₈ (EVAKYLLQNKAKVNAKAK) (E) AnkyrinR₆₁₆₋₆₃₃ (EVARSLLQYGGSSANAESV) (F) AnkyrinR₇₁₅₋₇₃₂ (KLVKFLQHQADVNAKTK) were incubated in the presence of recombinant FIH and displayed a net +16 Da mass shift as determined by LC\MS.

Figure S2 Assignment of hydroxylation at N105 in AnkyrinR₉₂₋₁₀₉ (EVVRELVNYGANVNAQSQ). (A) MS/MS of the non-hydroxylated peptide. (B) MS/MS of the hydroxylated peptide. A +16 Da mass shift is observed in the b ion series appearing at b₁₄, assigning hydroxylation at N105.

Figure S3 Assignment of hydroxylation at N233 in AnkyrinR₂₂₀₋₂₃₇ (NVAQLLLNRGSSVNFTPQ). (A) MS/MS of the non-hydroxylated peptide. (B) MS/MS of the hydroxylated peptide. A +16 Da mass shift is observed in the b ion series appearing at b₁₄, assigning hydroxylation at N233.

Figure S4 Assignment of hydroxylation at N464 in AnkyrinR₄₅₁₋₄₆₈ (EVAKYLLQNKAKVNAKAK). (A) MS/MS of the non-hydroxylated peptide. (B) MS/MS of the hydroxylated peptide. A +16 Da mass shift is observed in the y ion series appearing at y₅, assigning hydroxylation at N464.

Figure S5 Assignment of hydroxylation at N629 in AnkyrinR₆₁₆₋₆₃₃ (EVARSLLQYGGSSANAESV). Insets are regions expanded from the main spectra. (A) MS/MS of the non-hydroxylated peptide. (B) MS/MS of the hydroxylated peptide. A +16 Da mass shift is observed in the a ion and b ion series appearing at a₁₄ and b₁₄, assigning hydroxylation at N629.

Figure S6 Assignment of hydroxylation at N728 in AnkyrinR₇₁₅₋₇₃₂ (FLLQHQADVNAK). (A) MS/MS of the non-hydroxylated tryptic fragment. (B) MS/MS of the hydroxylated tryptic fragment. A +16 Da mass shift is observed in the y ion series appearing at y₃, assigning hydroxylation at N728.

Figure S7 Peptide fragments derived from human ankyrinB are FIH substrates. (A) The sequences of the 24 ARs of human ankyrinB were aligned to the consensus sequence by Michaely *et al.* (1). Ψ indicates a non-polar residue. Repeat numbers are on the left and amino acid residue numbers on the right. Underlined are sequences of peptide fragments synthesized to encompass the Asn- and Asp-residues at the conserved hydroxylation position with the absence of a prolyl residue at the -1 position. An * indicates peptides observed to be FIH substrates. The predicted asparaginyl hydroxylation sites are highlighted in bold and their residue numbers given in parenthesis on the right. (B) MALDI-TOF spectra of the ankyrinB peptide fragments after incubation with FIH under standard assay conditions.

For peptide containing N58, N124, N656 and N755, a +16 Da mass shift was observed after incubation with FIH, consistent with hydroxylation.

Figure S8 Peptide fragments derived from human ankyrinG are FIH substrates. (A) The sequences of the 24 ARs of human ankyrinG were aligned to the consensus sequence by Michaely *et al.* (1). Ψ indicates a non-polar residue. Repeat numbers are on the left and amino acid residue numbers on the right. Underlined are sequences of peptide fragments synthesized to encompass the Asn- and Asp-residues at the conserved hydroxylation position with the absence of a prolyl residue at the -1 position. An * indicates peptides observed to be FIH substrates. The predicted asparaginyl hydroxylation sites are highlighted in bold and their residue numbers given in parenthesis on the right. (B) MALDI-TOF spectra of the ankyrinG peptide fragments after incubation with FIH under standard assay conditions. For peptide containing N68, N134, N658, N691 and N757, a +16 Da mass shift was observed after incubation with FIH, consistent with hydroxylation.

Figure S9 MS/MS assignment of hydroxylation at N431 in D34 co-expressed with FIH in *E. coli*. (A) MS/MS of the non-hydroxylated 427-436 tryptic peptide GASP NVSNVK. (B) MS/MS of the hydroxylated 427-436 tryptic peptide derived from D34 co-expressed with FIH in *E. coli*. A +16 Da mass shift is observed in the y ion series appearing at y_6 , assigning hydroxylation at N431.

Figure S10 MS/MS assignment of hydroxylation at N464 in D34 co-expressed with FIH in *E. coli*. (A) MS/MS of the non-hydroxylated 452-469 endoproteinase Glu-C digested peptide fragment VAKYLLQNKAKVNAKAKDD. (B) MS/MS of the hydroxylated 452-469 fragment derived from D34 co-expressed with FIH in *E. coli*. A +16 Da mass shift is observed in the y ion series appearing at y_7 , assigning hydroxylation at N464.

Figure S11 MS/MS assignment of hydroxylation at N629 in D34 co-expressed with FIH in *E. coli*. (A) MS/MS of the non-hydroxylated SLLQYGG SANAESVQGV TPLHLAAQEGHAEMVALLLSK 620-657 tryptic peptide. (B) MS/MS of the hydroxylated 620-657 tryptic peptide derived from D34 co-expressed with FIH in *E. coli*. A +16 Da mass shift is observed at the b ion series appearing at b_{10} and y ion series appearing at y_{29} , assigning hydroxylation at N629.

Figure S12 MS/MS assignment of hydroxylation at N662 in D34 co-expressed with FIH in *E. coli*. (A) MS/MS of the non-hydroxylated 658-666 tryptic peptide QANGNLGNK. (B) MS/MS of the hydroxylated 658-666 tryptic peptide derived from D34 co-expressed with FIH in *E. coli*. A +16 Da mass shift is observed in the y ion series appearing at y_5 and b^* ions (b ions with ammonium loss) at b_5^* , assigning hydroxylation at N662.

Figure S13 MS/MS assignment of hydroxylation at N728 in D34 co-expressed with FIH in *E. coli*. (A) MS/MS of the non-hydroxylated 719-730 tryptic peptide FLLQH QADVNAK. (B) MS/MS of the hydroxylated 719-730 tryptic peptide derived from D34 co-expressed with FIH in *E. coli*. A +16 Da mass shift is observed in the y ion series appearing at y_3 , assigning hydroxylation at N728.

Figure S14 MS/MS assignment of hydroxylation at N761 in D34 co-expressed with FIH in *E. coli*. (A) MS/MS of the non-hydroxylated 756-775 tryptic peptide NGASPNEVSSDGTPLAIK. (B) MS/MS of the hydroxylated 756-775 tryptic peptide derived from D34 co-expressed with FIH in *E. coli*. A +16 Da mass shift is observed in the y ion series appearing at y_{15} , assigning hydroxylation at N761.

Figure 15 FIH hydroxylates an aspartyl residue D695 in D34. (A1) LC/MS spectrum showing the unmodified 690-699 (HGVMVDATTR) tryptic fragment ($[M+2H]^{2+} = m/z$ 543.7) containing D695. (A2) MS/MS analysis of $m/z = 543.7$, assigning the sequence of the 690-699 tryptic peptide. (B1) LC/MS spectrum showing the M693-oxidized ($[M+2H]^{2+} = m/z$ 551.7) 690-699 tryptic peptide. (B2) MS/MS of $m/z = 551.7$, assigning oxidation at M693. A -48 Da shift is observed in the y ion series appearing at y_7 , corresponding to fragments containing M693. The -48 Da mass shift is consistent with M693 first being oxidized (+16 Da) and then undergoing collision induced dissociation (CID) via sulfoxide elimination, resulting in a neutral weight loss of 64 Da and the release of

methanesulfenic acid. (C1) LC/MS spectrum showing the M693-oxidized and D695-hydroxylated ($[M+2H]^{2+} = m/z$ 559.7) 690-699 tryptic peptide. (C2) MS/MS of $m/z = 559.7$. A +16 Da mass shift is observed in the y ion series appearing at y_5 compared to corresponding y ions in (B2), assigning hydroxylation at D695.

Figure S16 The ankyrinB ARD is a substrate for multiple FIH-catalysed Asn-hydroxylations. Pure recombinant ankyrinB ARD was incubated in the absence or presence of FIH under standard assay conditions, followed by SDS-PAGE analyses and trypsinolysis. The resultant in-gel digests were subjected to MS analyses. (A) LC/MS spectra showing the non-hydroxylated and partially hydroxylated forms of the (i) 53-73 (GGIDINTCNQNGLNALHLAAK), (ii) 119-147 (EGANINAQSQNGFTPLYMAAQENHIDVVK) and (iii) 640-660 (NQMQUIASTLLNYGAETNIVTK) tryptic peptides. (B) MS/MS analyses of the non-hydroxylated and hydroxylated 640-660 tryptic fragment assigning hydroxylation at N656. A +16 Da mass shift is observed in the y ion series appearing at y_5 , assigning hydroxylation at N656.

Figure S17 FIH hydroxylates an aspartyl residue D491 in the ankyrinB ARD. (A) LC/MS (A1) and MS/MS (A2) spectra of the unmodified 486-493 (NGALVDAR) tryptic peptide. (B) LC/MS (B1) and MS/MS (B2) spectra of the hydroxylated (~15%) 486-493 tryptic peptide. A +16 Da mass shift is observed in the y ion series appearing at y_3 compared to the unmodified peptide, assigning hydroxylation to D491.

Figure S18 D34 is hydroxylated in HEK293T cells overexpressing wildtype FIH. V5-tagged D34 immunopurified from HEK293T cells co-transfected in the presence or absence of FIH were subjected to trypsin digestion followed by MS analyses. (A-D) LC/MS spectra showing the non-hydroxylated and partially hydroxylated forms of the (A) 427-436 (GASPNVSNVK), (B) 620-657 (SLLQYGGSSANAESVQGVTPHLHLAAQEGHAEMVALLLSK), (C) 719-730 (FLLQHQADVNAK) and (D) 756-775 (NGASPNEVSSDGTTPPLAIK) tryptic peptides. (E) LC/MS spectra showing the unmodified ($[M+2H]^{2+} = m/z$ 543.8), M693-oxidized ($[M+2H]^{2+} = m/z$ 551.8), and M693-oxidized as well as D695-hydroxylated ($[M+2H]^{2+} = m/z$ 559.8) forms of the 690-699 (HGVMVDATTR) tryptic peptide. Mox stands for methionine oxidation.

Figure S19 MS/MS assignment of hydroxylation at N431 in D34 co-expressed with FIH in 293T cells. (A) MS/MS of the non-hydroxylated 427-436 tryptic peptide GASPNVSNVK. (B) MS/MS of the hydroxylated 427-436 tryptic peptide. A +16 Da mass shift is observed in the y ion series appearing at y_6 , assigning hydroxylation at N431.

Figure S20 MS/MS assignment of hydroxylation at N629 in D34 co-expressed with FIH in 293T cells. (A) MS/MS of the non-hydroxylated 620-657 tryptic peptide SLLQYGGSSANAESVQGVTPHLHLAAQEGHAEMVALLLSK. (B) MS/MS of the hydroxylated 620-657 tryptic peptide. A +16 Da mass shift is observed at the y_{29} ion, consistent with hydroxylation at N629.

Figure S21 MS/MS assignment of hydroxylation at N728 in D34 co-expressed with FIH in 293T cells. (A) MS/MS of the non-hydroxylated 719-730 FLLQHQADVNAK tryptic peptide. (B) MS/MS of the hydroxylated 719-730 tryptic peptide. A +16 Da mass shift is observed in the y ion series appearing at y_3 , assigning hydroxylation at N728.

Figure S22 MS/MS assignment of hydroxylation at N761 in D34 co-expressed with FIH in 293T cells. (A) MS/MS of the non-hydroxylated NGASPNEVSSDGTTPPLAIK tryptic peptide. (B) MS/MS of the hydroxylated tryptic peptide. A +16 Da mass shift is observed in the y ion series appearing at y_{15} , assigning hydroxylation at N761.

Figure S23 MS/MS assignment of hydroxylation at D695 in D34 co-expressed with FIH in 293T cells. (A) MS/MS of the unmodified 690-699 tryptic peptide. (B) MS/MS of the M693-oxidized tryptic peptide, assigning oxidation at M693. A -48 Da shift is observed in the y ion series appearing at y_7 ,

corresponding to fragments containing M693. The -48 Da mass shift is consistent with M693 first being oxidized (+16 Da) and then undergoing collision induced dissociation (CID) via sulfoxide elimination, resulting in a neutral weight loss of 64 Da and the release of methanesulfenic acid. (C) MS/MS of the M693-oxidized and D695 hydroxylated tryptic peptide ($[M+2H]^{2+} = m/z$ 559.7). A +16 Da mass shift is observed in the y ion series appearing at y_5 compared to (B), assigning hydroxylation at D695.

Figure S24 LC/MS and MS/MS analyses demonstrating the oxidation at F795 in D34 immunopurified from HEK293T cells. (A, B) LC/MS spectra of the unoxidized and oxidized forms of the 788-801 VVTDETSFVLVSDK tryptic peptide derived from (A) D34 immunopurified from HEK293T cells and (B) D34 co-expressed with FIH in HEK293T cells. (C) MS/MS of the unoxidized peptide. (D) MS/MS of the oxidized peptide. A +16 Da mass shift is observed in the y ion series appearing at y_7 , assigning oxidation at F795.

Figure S25 N138, N233 and N728 in human endogenous ankyrinR are hydroxylated. LC/MS spectra of the (A) 129-169 tryptic peptide containing, (B) 229-248 tryptic peptide containing N233 and (C) 719-730 tryptic peptide show both hydroxylated unhydroxylated peaks. See Supplemental Figure S26 and S27 for MS/MS analyses assigning hydroxylation to N138 and N233, respectively.

Figure S26 MS/MS assignment of hydroxylation at N138 in human endogenous ankyrinR. Insets are regions expanded from the main spectra. (A) MS/MS of the unhydroxylated 129-169 tryptic peptide FLENGANQNVATEDGFTPLAVALQQGHENVVAHLINYGTK. (B) MS/MS of the hydroxylated 129-169 tryptic peptide. A +16 Da mass shift is observed in the b ion series appearing at b_{10} , assigning hydroxylation at N138.

Figure S27 MS/MS assignment of hydroxylation at N233 in human endogenous ankyrinR. (A) MS/MS of the unhydroxylated 229-248 GSSVNFTPQNGITPLHIASR tryptic peptide. Residue N238 is present in an Asn-Gly motif and Asn-deamidation at this site is observed, as presented for other such motifs (2). (B) MS/MS of the hydroxylated 229-248 tryptic peptide. In addition to deamidation at N238, a +16 Da mass shift is observed at the y_{16} ion, assigning hydroxylation at N233.

Figure S28 Mouse erythrocyte ankyrinR is hydroxylated. (A) Purification of ankyrinR from mouse erythrocytes. (Lane 1) Mw Marker. (Lane 2) Purification of human ankyrinR as described in Figure 5. (Lane 3 and 4) Purification of mouse ankyrinR following the same protocol as that for human. Arrow indicates where mouse ankyrinR was identified by MS analyses. (B) LC/MS spectrum showing the unhydroxylated and hydroxylated forms of the 96-110 tryptic fragment ELVNYGANVNAQSQ. (C) MS/MS of the unhydroxylated tryptic peptide. (D) MS/MS of the hydroxylated peptide. A +16 Da mass shift is observed in the y ion series appearing at y_6 , assigning hydroxylation at N105.

Figure S29 Conservation of the hydroxylation sites within the ankyrinR ARD in mammals. Protein sequences of mammalian ankyrinR ARDs were obtained from the UniProt Database, aligned using ClustalW software and shaded using the Boxshade Server (http://www.ch.embnet.org/software/BOX_form.html). Residues hydroxylated in endogenous and exogenous ankyrinR material purified from human cells are indicated by arrows

Figure S30 MS analyses demonstrating the oxidation at W1454 in human endogenous ankyrinR. (A) LC/MS (A1) and MS/MS (B1) of the unmodified 1437-1457 VENPNSLLEQSVALLNLWVIR tryptic peptide ($[M+2H]^{2+} = m/z$ 1204.1). (B) LC/MS (B1) and MS/MS (B2) of the 'singly oxidized' 1437-1457 tryptic peptide ($[M+2H]^{2+} = m/z$ 1212.1). A +16 Da mass shift is observed in the y ion series appearing at y_4 , corresponding to fragments containing W1454. The mass increase is consistent with oxidation of tryptophan to hydroxytryptophan. Wox stands for hydroxytryptophan. (C) LC/MS (C1) and MS/MS (C2) of the 'doubly oxidized' 1437-1457 tryptic peptide ($[M+2H]^{2+} = m/z$ 1220.1). A +16 Da mass shift is observed in the y ion series appearing at y_4 compared to corresponding y ions in (B1). The mass increase is consistent with oxidation of hydroxytryptophan to N-formylkynurenine. NFK stands for N-formylkynurenine.

Figure S31 Hydroxylation modulates the interaction of D34 and CDB3. Coomassie-stained SDS-PAGE gel showing the *in vitro* pull-down of CDB3 (a.a. 2-379) using GST-D34, GST-D34-OH or control protein GST-ORF15 (3) as bait. Assays were performed as described previously (4).

Figure S32 Number of appearances for each amino acid at the conserved hydroxylation position. A total of 1505 human AR sequences were obtained from The SMART (<http://smart.embl.de/>), PFAM (<http://www.pfam.org>) and Uniprot (<http://www.uniprot.org>) databases, amongst which 1354 ARs with a length of 32, 33 or 34 residues were aligned and analysed.

Figure S33 Comparing the efficiency of FIH-catalysed Asn- and Asp-hydroxylation in a consensus AR sequence. All four synthetic AR peptides were incubated with FIH under identical assay conditions for 30 minutes, followed by MALDI-TOF analyses. All assays were carried out in duplicate.

Figure S34 FIH D201G variant does not catalyse aspartyl hydroxylation of Peptide 2. MALDI-TOF analyses of Peptide 2 (HLEVVKLLLEHGADVDAQDK) after incubation with either wildtype FIH (A) or FIH D201G variant (B) under identical assay conditions.

Figure S35 MS/MS assignment of hydroxylation at D1380 in the HLDVVQLLVOAGADVDAADN GTAR₁₃₆₅₋₁₃₈₄ peptide. (A) MS/MS of the unmodified peptide. (B) MS/MS of the hydroxylated peptide. A +16 Da mass shift is observed in the b ion series appearing at b₁₆, assigning hydroxylation at D1380.

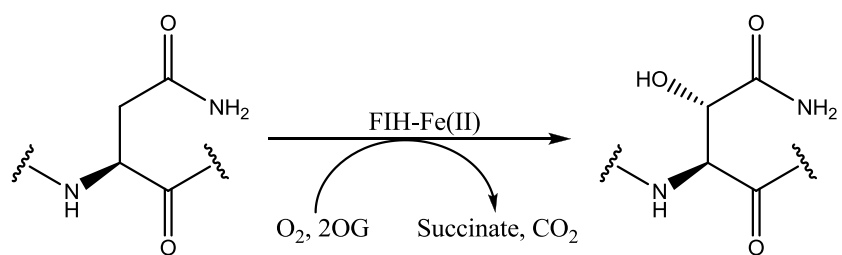
Figure S36 FIH Q239H variant displays aspartyl hydroxylase activity. MALDI-TOF analyses of Peptide 2 (HLEVVKLLLEHGADVDAQDK) after incubation with (A) Fe(II) and 2OG only, (B) wt FIH, Fe(II) and 2OG and (C) FIH Q239H, Fe(II) and 2OG under the same incubation conditions.

Figure S37 Crystal Structure of D34 with the hydroxylation sites highlighted. PDB code 1N11 (1).

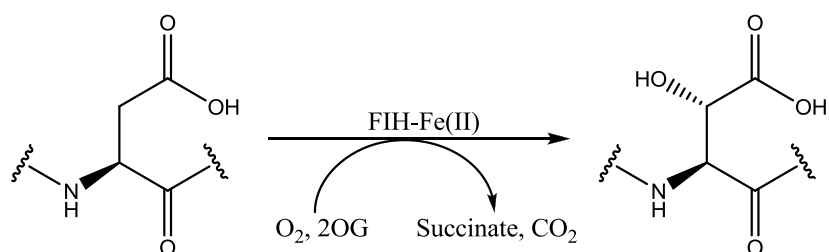
References

1. Michaely, P., Tomchick, D. R., Machius, M., and Anderson, R. G. (2002) *EMBO J* **21**, 6387-6396
2. Wakankar, A. A., and Borchardt, R. T. (2006) *J Pharm Sci* **95**, 2321-2336
3. Mackenzie, A. K., Valegard, K., Iqbal, A., Caines, M. E., Kershaw, N. J., Jensen, S. E., Schofield, C. J., and Andersson, I. *J Mol Biol* **396**, 332-344
4. Su, Y., Ding, Y., Jiang, M., Jiang, W., Hu, X., and Zhang, Z. (2006) *Mol Cell Biochem* **289**, 159-166

Supplemental Scheme 1 FIH catalysed asparaginyl hydroxylation.



Supplemental Scheme 2 FIH catalysed aspartyl hydroxylation.



Supplemental Table S1 Refinement statistics for crystal structure

Measurement	FIHQ239H.AnkR(Asp)
Data Collection	
Space Group	<i>P4₁2₁2</i>
Cell dimensions a,b,c (Å)	86.352 86.352 144.533
Resolution (Å)	74.12 - 2.20 (2.28 - 2.20)*
No. of unique reflections	26863
Completeness (%)	99.13 (97.16)*
Redundancy	9.2 (8.4)
R _{sym} **	0.071 (0.880)*
Mean I/σ(I)	28.48 (2.22)
Refinement	
R _{factor}	0.202
R _{free}	0.232
R.m.s. deviation	
Bond length, Å	0.009
Bond angle, °	1.049
No. of atoms	
Protein	2842
Peptide	138
Ligand (NOG)	10
Water	135
<B _{factor} >Å ²	
Protein	47.369
Peptide	45.735
Ligand (NOG)	44.542
Metal (Zn)	45.740
Water	48.134

*Highest resolution shell shown in parenthesis

**R_{sym} = $\sum |I - \langle I \rangle| / \sum I$, where *I* is the intensity of an individual measurement and $\langle I \rangle$ is the average intensity from multiple observations.

Supplemental Table S2 AR peptides tested as substrates for FIH-catalysed aspartyl hydroxylation. Peptides were incubated with FIH under standard assay conditions (see methods) and analysed by MALDI MS analyses. Hydroxylation was identified by observation of a clear +16 Da mass shift and verified by MSMS analyses (Figure 4D and Figure S21).

Peptide sequence	Swiss-Prot Accession	Swiss-Prot locus	Mass	Hydroxylation identified
HVEVVSELLQREANVDAATK	Q12955	ANK3 (86-105)	2208.4	×
HF'DVVQLLVQAGADVDAADN	Q8IWZ3	ANKH1 (1337-1356)	2097.3	✓
DDGTARLLLDHGACVDAQER	Q8NFD2	ANKK1 (440-459)	2155.5	×
HEIIVQYFLNHGKVDARDH	Q6ZW76	ANKS3 (181-200)	2390.7	×
GVQIVELLLLHAITDVEDAKAS	Q9P2S6	ANKY1 (597-616)	2092.6	×
HL'DVVQLLVQAGADVDAADN	O75179	ANR17 (1365-1384)	2063.3	✓
HTDCVYSLLNKGANVDAKDK	O15084	ANR28 (698-717)	2191.6	×
QARCVQLLLAAGAQVDARNI	Q8WXX3	ASB13 (64-83)	2110.6	×
ELIRVILKTSKPKDVEDATCS	Q8N3C7	CLIP4 (164-183)	2216.8	×
HVSTVKLLLENNAQVEDATDV	Q9Y283	INVS (369-388)	2166.4	×
QVEVVRCLLRNGALVEDARAR	Q01484	ANK2 (476-495)	2238.7	×
RVNVAEVLVNQGAHVDAQTK	Q12955	ANK3 (709-728)	2148.3	×
HSQLVNKLLVAGATVDARDL	Q86SG2	ANR23 (156-175)	2120.6	×
HVPVITTLRGGARVDALDR	Q6NXT1	ANR54 (188-207)	2159.7	×
LDEHARLYLGRGAHVDAARNG	Q6ZVZ8	ASB18 (231-250)	2220.7	×
ERGLVQFLLQAGAQVDARML	O00221	IKBE (413-432)	2215.9	×
REVCQLLLRSRQTAVDARTE	Q99466	NOTC4 (1680-1699)	2344.7	×
YTEMVALLLEFGANVDASSE	Q9HCD6	TANC2 (897-916)	2159.7	×
NYVKVKIKLKKGIYVDAVNS	Q8IWB6	TEX14 (35-54)	2280.0	×
HL'SCLQVLLAHGADVDSL'DV	Q8WXX4	ASB12 (76-95)	2105.5	×
RTELLHDLVQHVS'DVEDA	Q8IYU2	HACE1 (143-162)	2290.4	×
RADILKALIRYGADV'DVNHH	Q9Y576	ASB1 (156-175)	2276.8	×

Figure S1

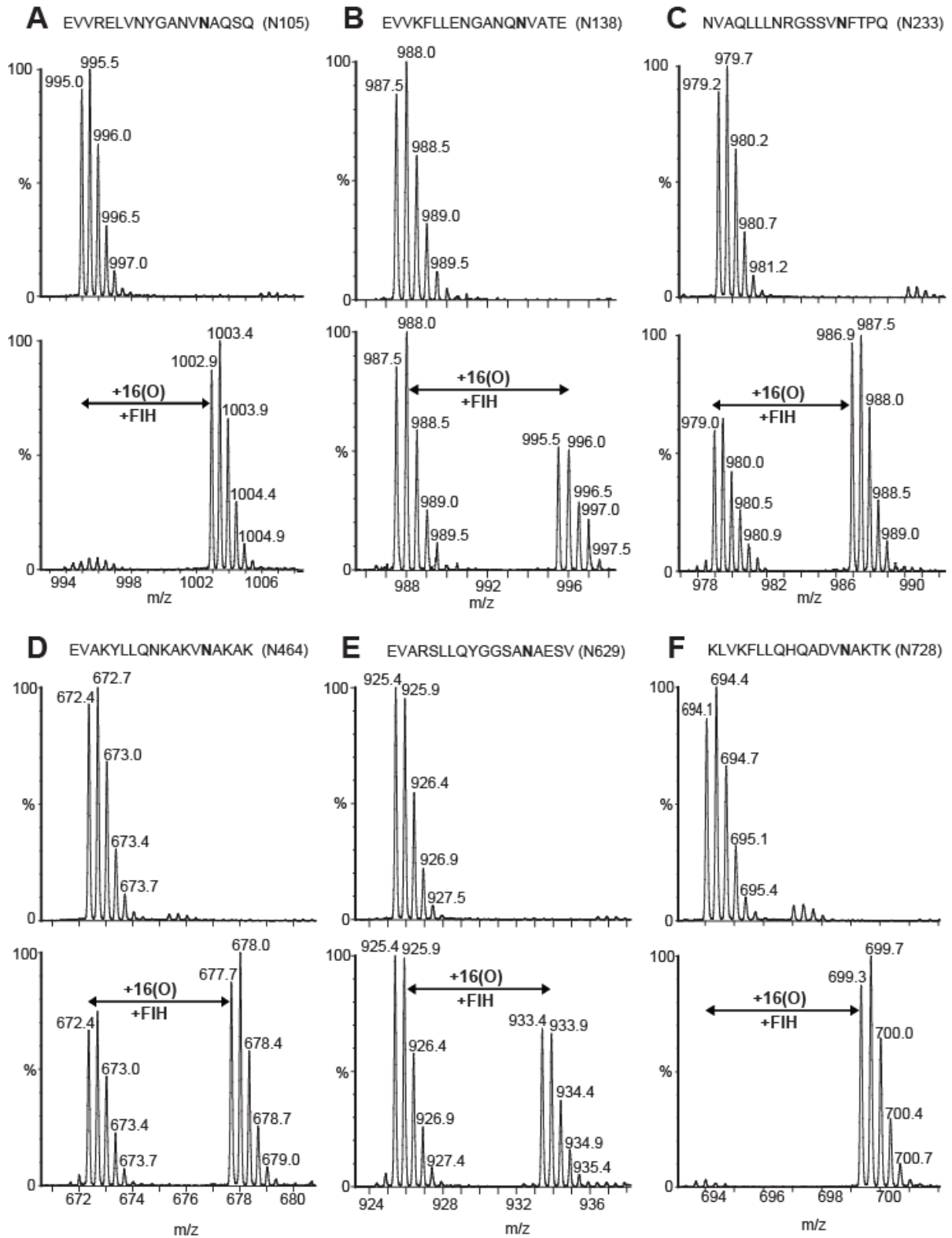


Figure S2

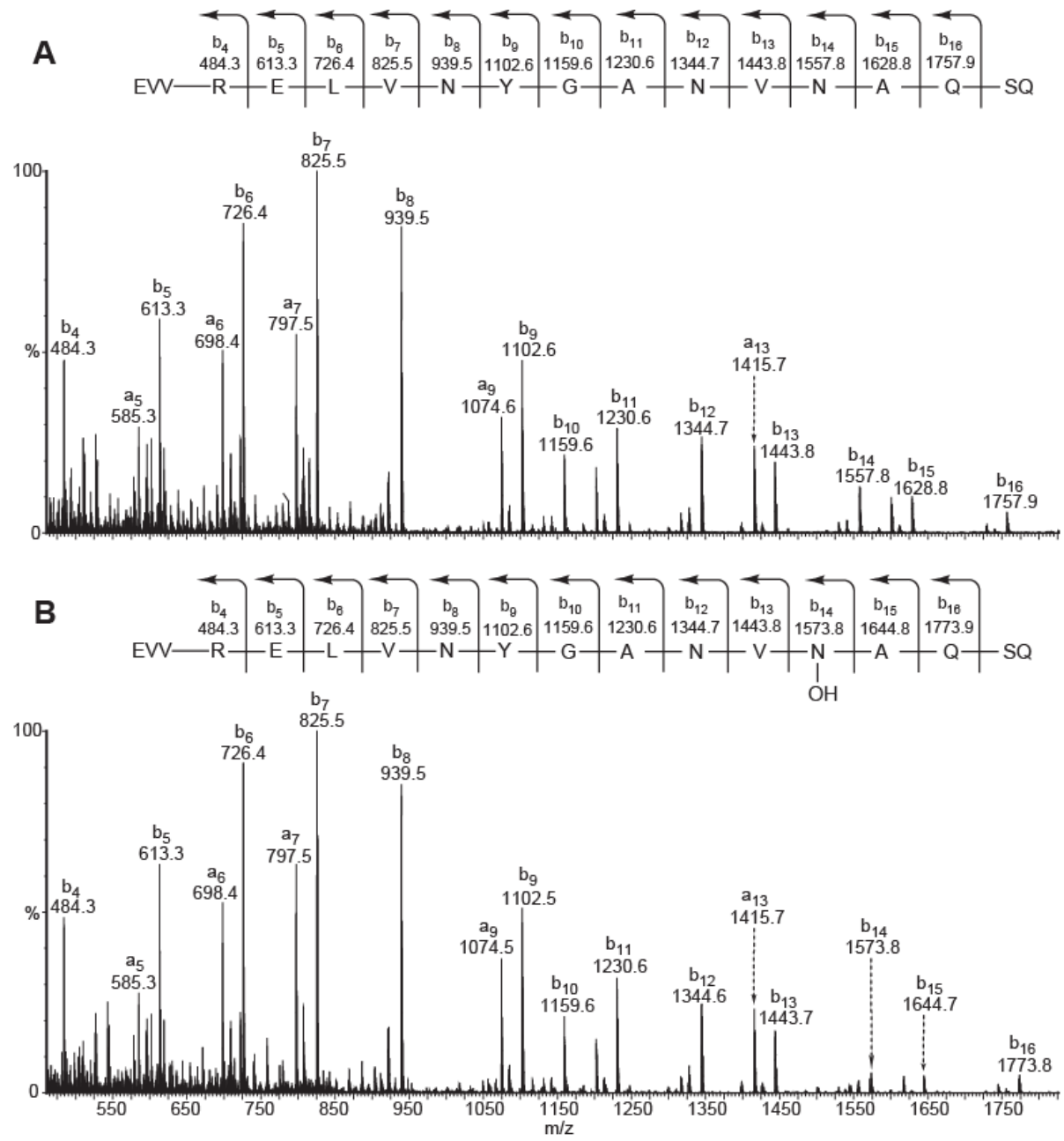


Figure S3

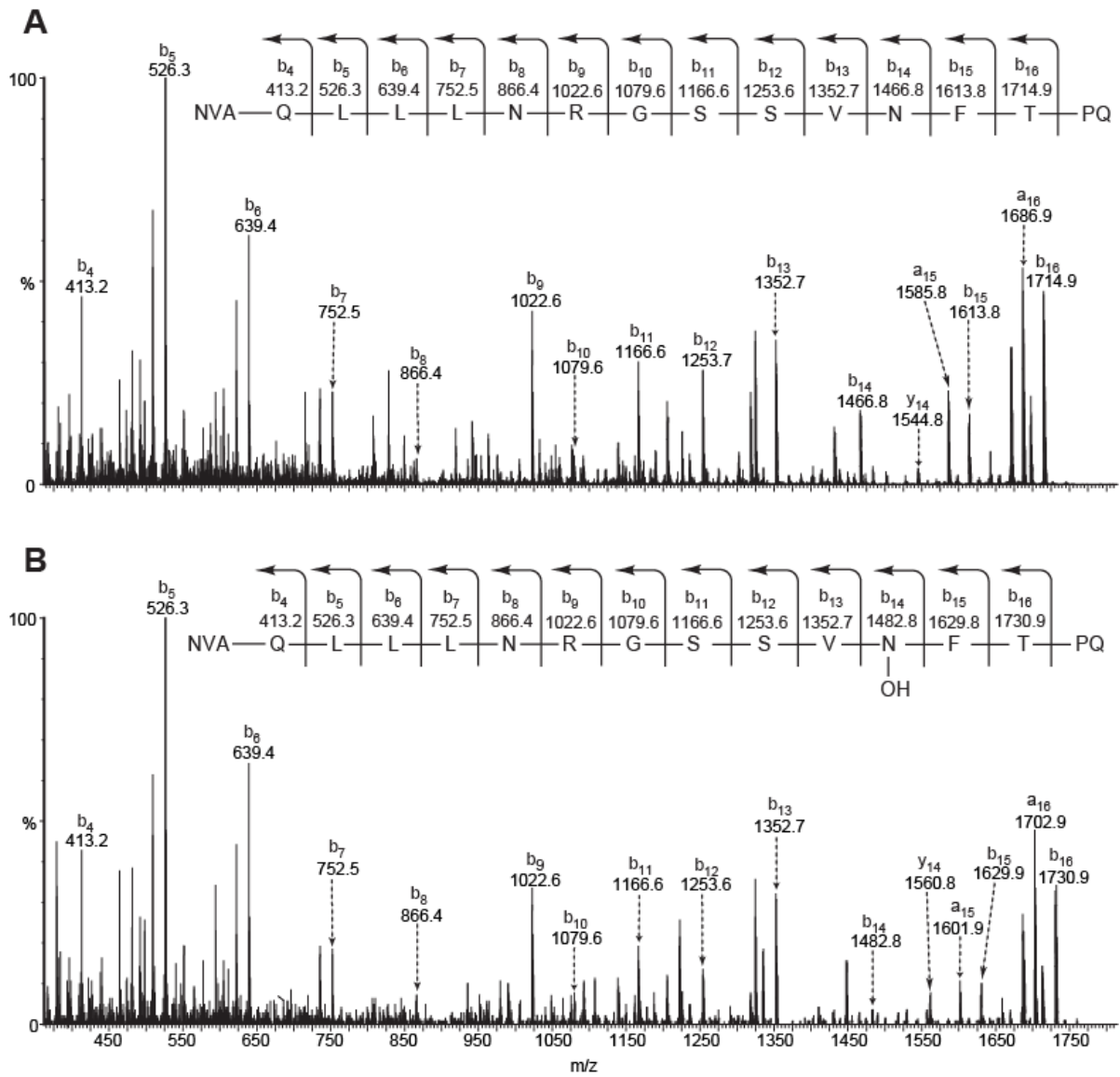


Figure S4

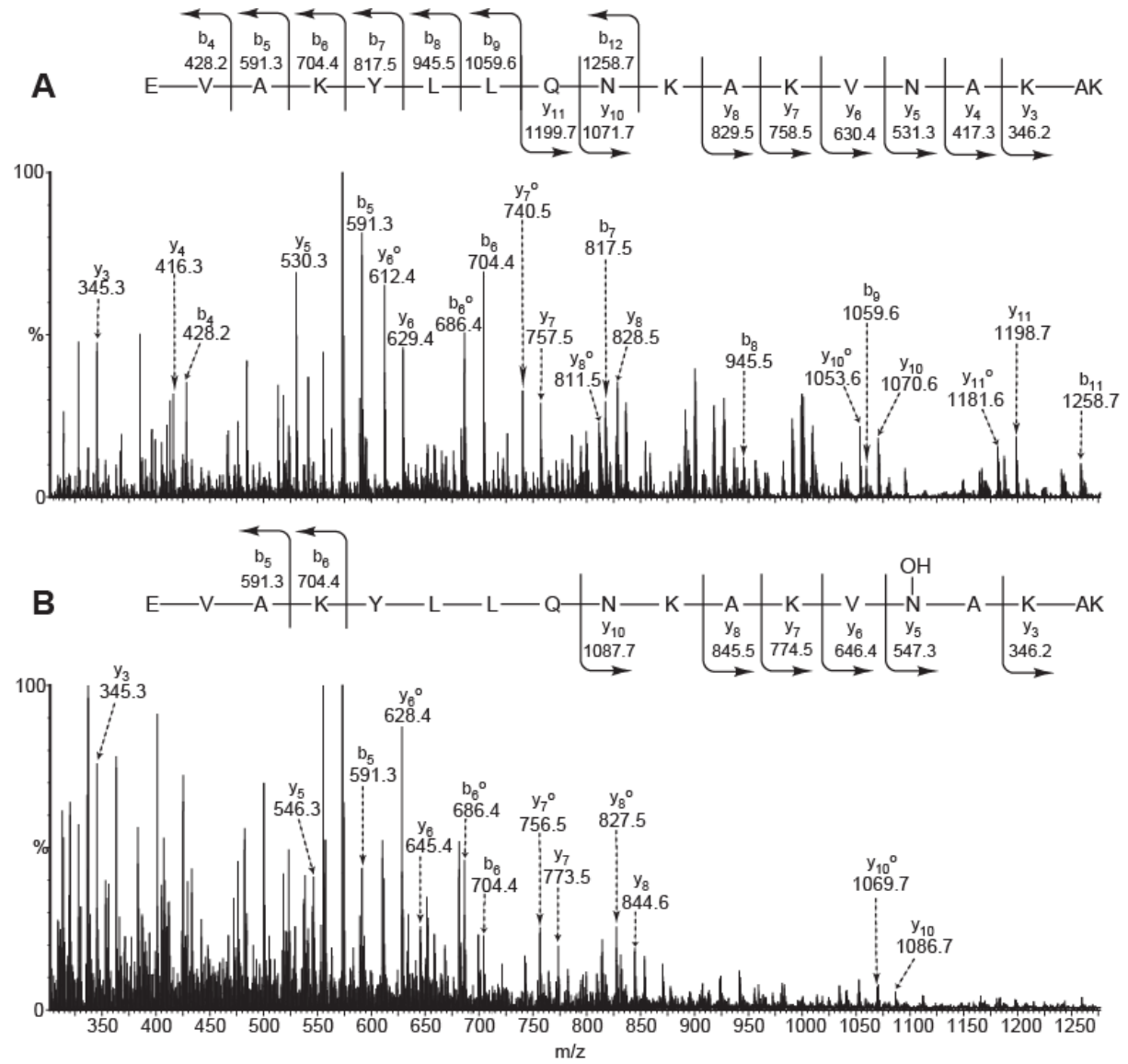


Figure S5

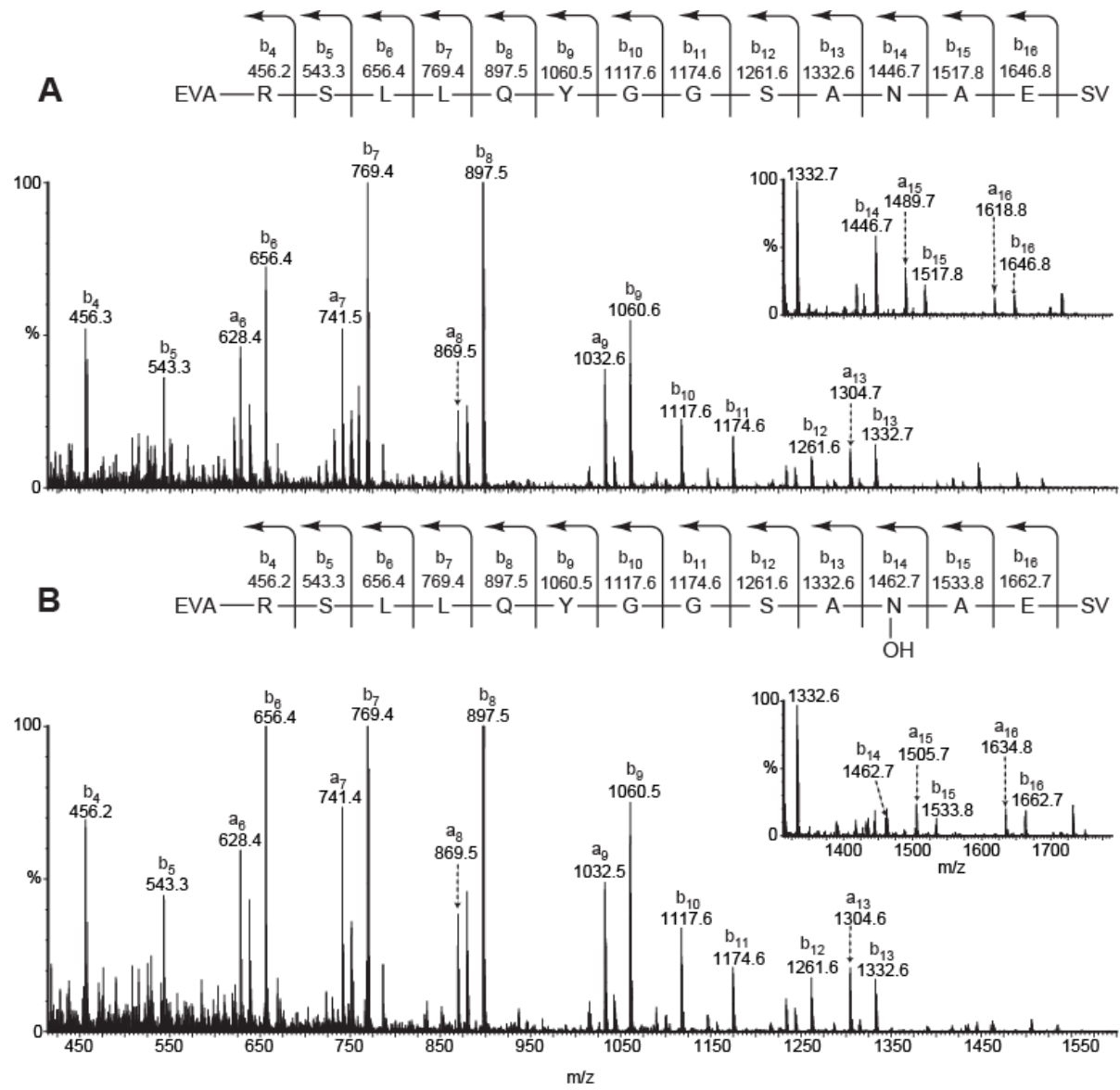


Figure S6

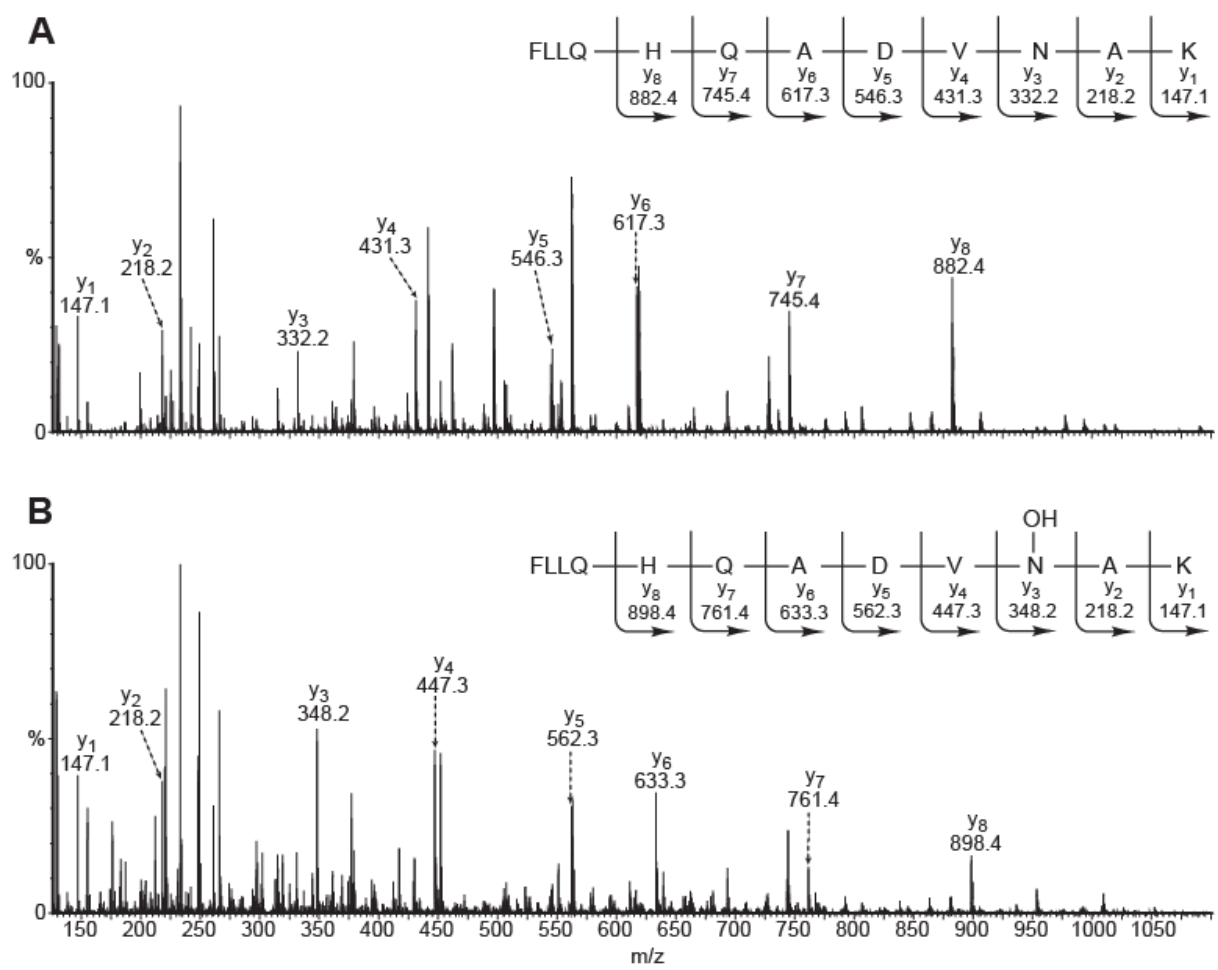


Figure S7

A

		
Consensus	-G-TPLHΨAA--GH--ΨV-ΨLL--GA--N----	
Repeat 1	DSNASFLRAARAGNLDKVVVEYLKGGIDINTCNO*	62 (N58)
Repeat 2	NGLNALHLAAKEGHVGLVQELLGRGSSVDSATK	95
Repeat 3	KGNTALHIASLAGQAEVVKVLVKEGANINAQSQ*	128 (N124)
Repeat 4	NGFTPLYMAAQENHIDVVKYLLENGANQSTATE	161
Repeat 5	DGFTPLAVALQQGHNQAVAILLENDTKG K	190
Repeat 6	VRLPALHIAARKDDTKSAALLLQNDHNADVQSKMMVNRTE	231
Repeat 7	SGFTPLHIAAHYGNVNVATLLNLRGAAVDFTAR	264
Repeat 8	NGITPLHVASKRGNTNMVKLLLRGGQIDAKTR	297
Repeat 9	DGLTPLHCAARSGHDQVVELLLERGAPELLARTK	330
Repeat 10	NGLSPLHMAAQGDHVECVKHLLOHKAPVDDVTL	363
Repeat 11	DYLTALHVAACHCGHYRVTKLLLDKRAPNARAL	396
Repeat 12	NGFTPLHIACKKNRIKVMELLVKYGASIQAITK	429
Repeat 13	SGLTPIHVAAFMGHLNIVLLLLQNGASPDVTNI	462
Repeat 14	RGETALHMAARAGQVEVVRCLLRNGALVDARAR	495
Repeat 15	EEQTPLHIASRLGKTEIVQLLLQHMAHPDAATT	528
Repeat 16	NGYTPLHISAREGQVDVASVLEAGAAHSLATK	561
Repeat 17	KGFTPLHVAAKYGLDVAKLLLRRAAADSAGK	594
Repeat 18	NGLTPLHVAAHYDNQKVALLLLEKASPHATAK	627
Repeat 19	NGYTPLHIAAKKNQMQIAS ^T LLNYGAETNIVTK*	660 (N656)
Repeat 20	QGVTPHLHLASQEGHTDMVTLLLDKGANIHMSTK	693
Repeat 21	SGLTSLHLAAQEDKVNVDILTKHGADQDAHTK	726
Repeat 22	LYTPLIVACHYGNVVMVNFLLKQGANVNAKTK*	759 (N755)
Repeat 23	NGYTPLHQAAQQGH ^T HIINVLLQHGAKPNATTA	792
Repeat 24	NGNTALAIAKRLGYISVVDTLKVVTEEVTTTTT	825

B

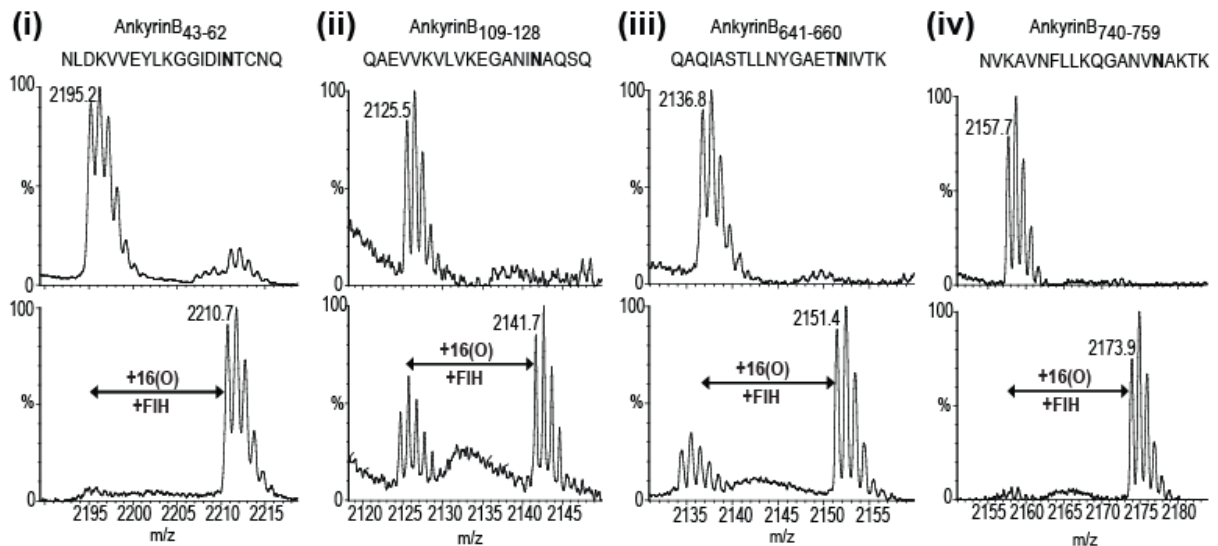



Figure S8

A

			
Consensus	-G-TPLHWAA--GH--WV-ΨLL--GA--N----		
Repeat 1	DANASYLRAARAGHLEKALDYIKNGVDINICNQ *	72	(N68)
Repeat 2	NGLNALHLASKEGHVEVVSSELLQREANVDAATK	105	
Repeat 3	KGNTALHIASLAGQAEVVKVLVTNGANVNAQSQ *	138	(N134)
Repeat 4	NGFTPLYMAAQENHLEVVKFLLDNGASQSLATE	171	
Repeat 5	DGFTPLAVALQQGHDQVVSLLLENDTKG K	200	
Repeat 6	VRLPALHIAARKDDTKAAALLLQNDNNADVESK	233	
Repeat 7	SGFTPLHIAAHYGNINVATLLLNRAAAVDFTAR	266	
Repeat 8	NDITPLHVASKRGNANMVKLLLDRGAKIDAKTR	299	
Repeat 9	DGLTPLHCGARSGHEQVVEMLLDRAAPILSKTK	332	
Repeat 10	NGLSPLHMATQGDHLNCVQLLLQHNVPVDDVTN	365	
Repeat 11	DYLTALHVAACHGHYKVAKVLLDKKANPNAKAL	398	
Repeat 12	NGFTPLHIACKNRKIKVMELELLKHGASIQAVTE	431	
Repeat 13	SGLTPIHVAAFMGHVNIVSQMLMHGASPNTTNV	464	
Repeat 14	RGETALHMAARSGQAEVVRYLVQDGAQVEAKAK	497	
Repeat 15	DDQTPLHISARLGKADIVQQLLQQGASPNAATT	530	
Repeat 16	SGYTPLHLSAREGHEDVAAFLLDHGASLSITTK	563	
Repeat 17	KGFTPLHVAAKYGKLEVANLLLQKSASPDAAGK	596	
Repeat 18	SGLTPLHVAAHYDNQKVALLLLDQGASPHAAAK	629	
Repeat 19	NGYTPLHIAAKNQMDIATTLLEYGADANAVTR *	662	(N658)
Repeat 20	QGIASVHLAAQEGHVDMSVLLLRNANVNLSNK *	695	(N691)
Repeat 21	SGLTPLHLAAQEDRVNVAEVLVNQGAHVDAQTK	728	
Repeat 22	MGYTPLHVGCHYGNIKIVNFLLQHSAKVNAKTK *	761	(N757)
Repeat 23	NGYTPLHQAAQQGHTHINVLLQNNASPNELTV	794	
Repeat 24	NGNTALGIARRLGYISVVDTLKIVTEETMTTTT	827	

B

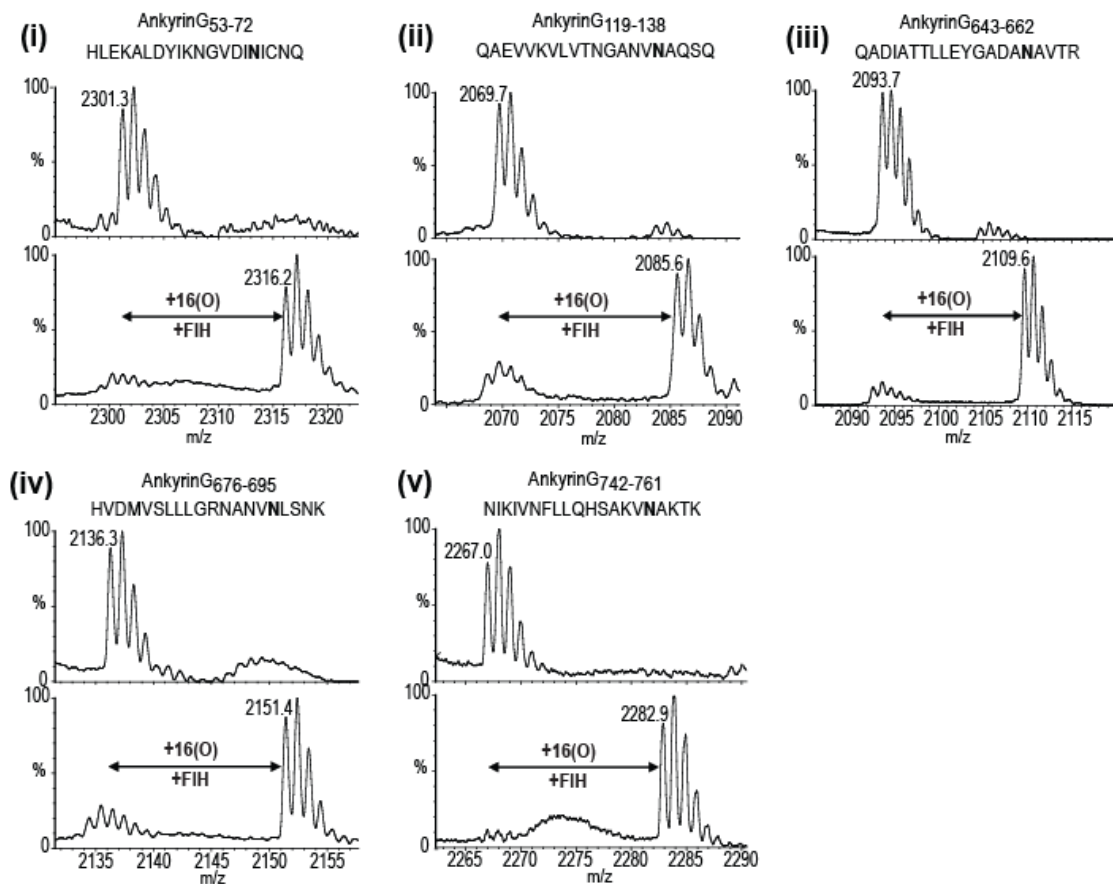


Figure S9

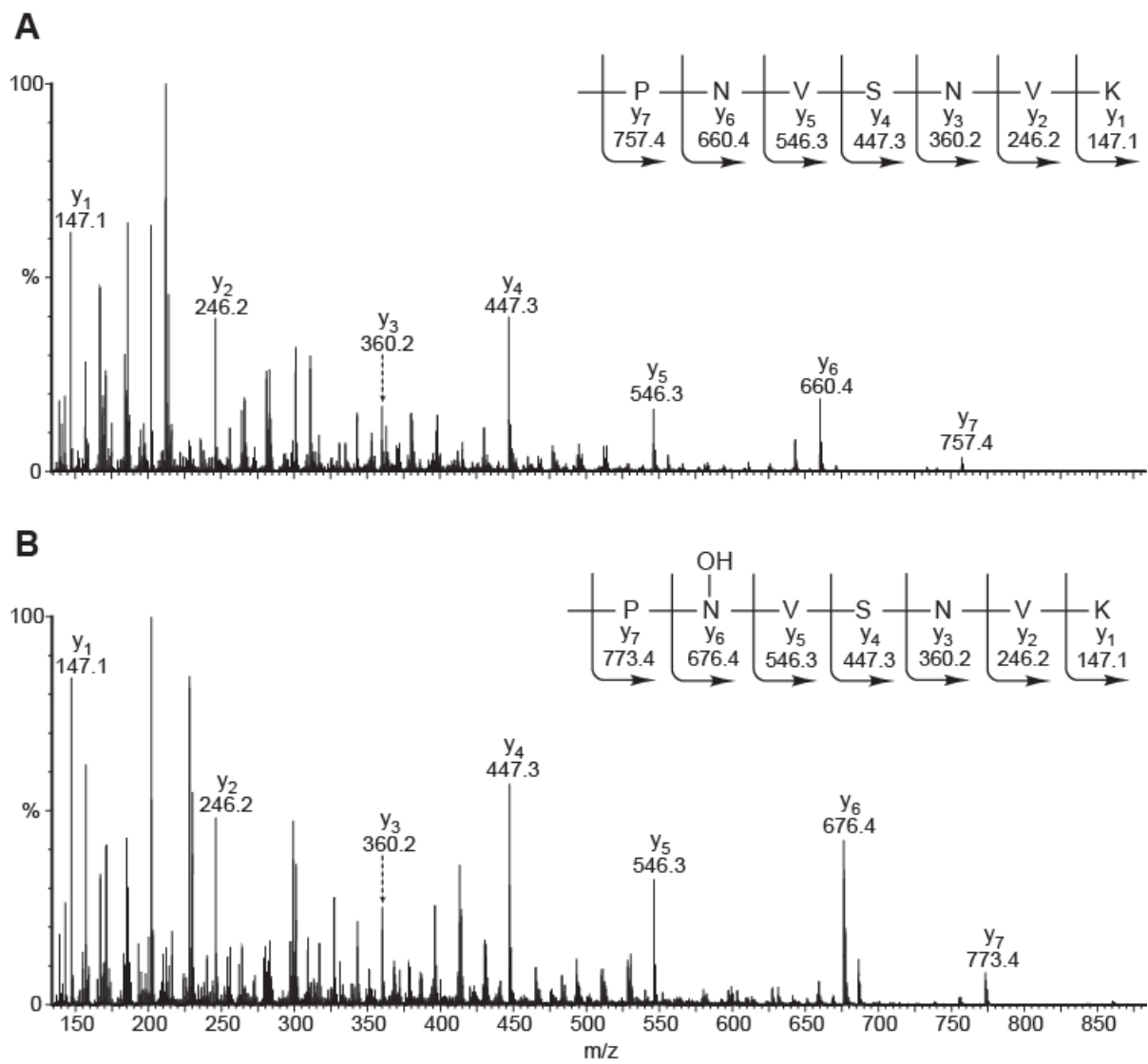


Figure S10

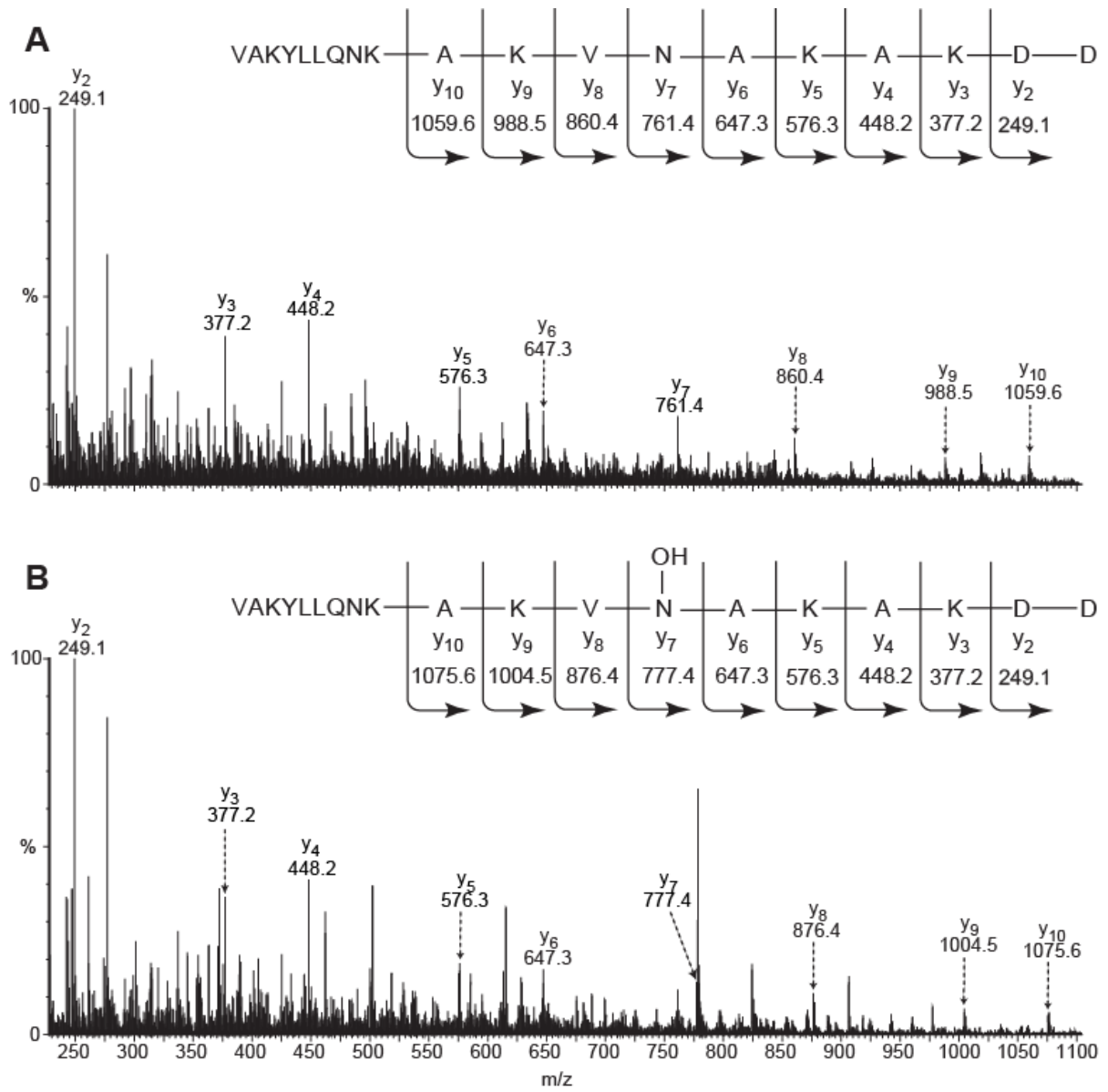


Figure S11

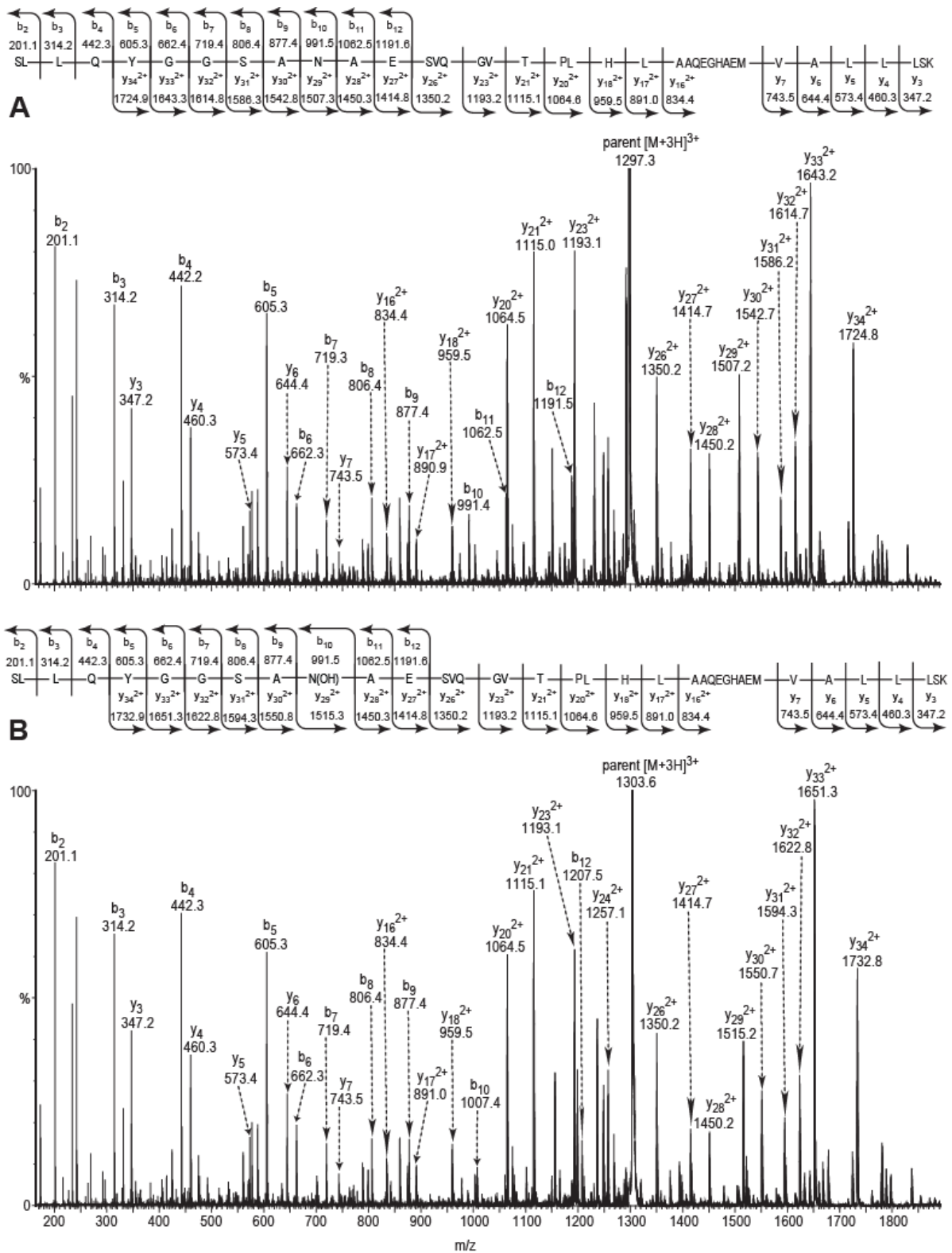


Figure S12

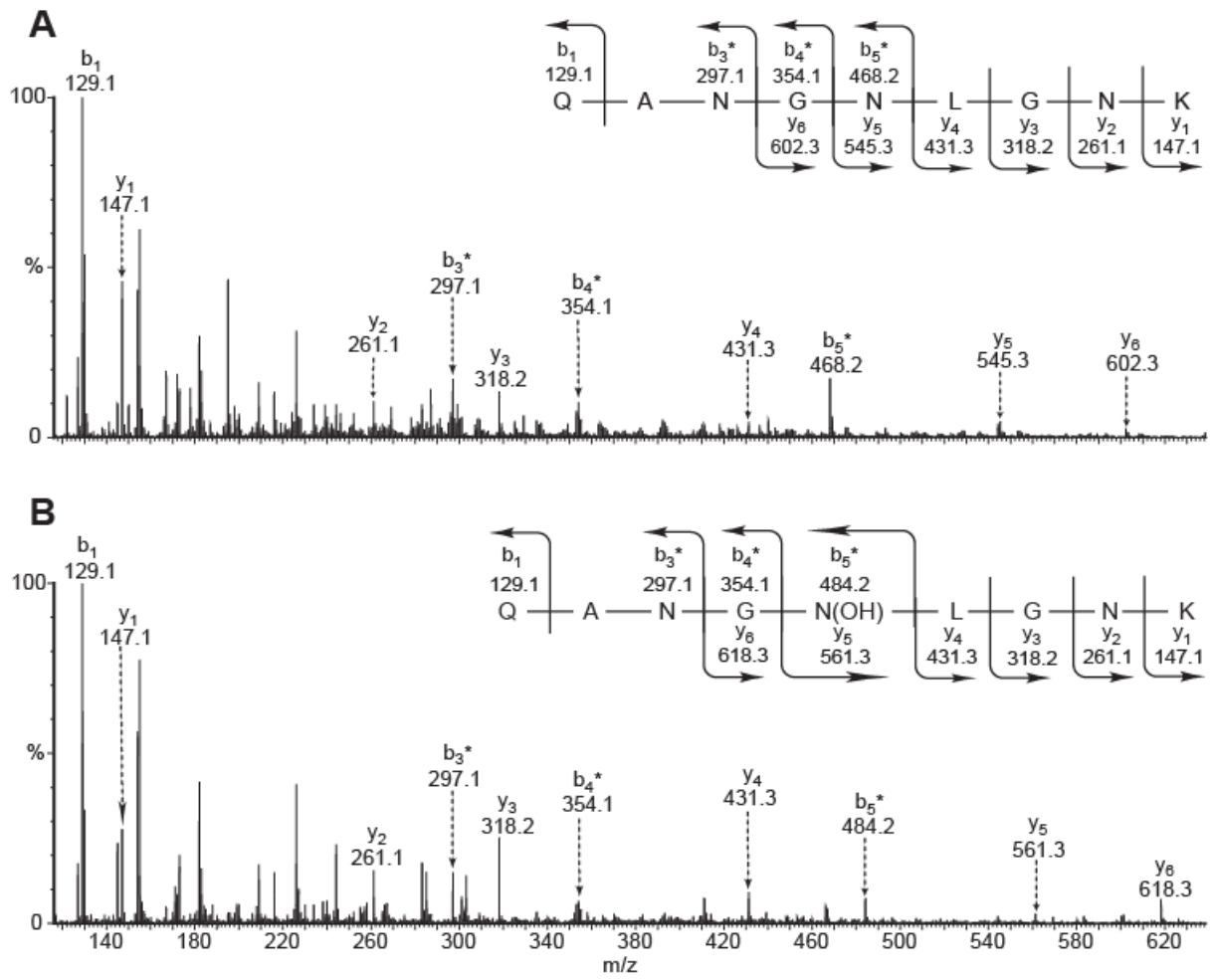


Figure S13

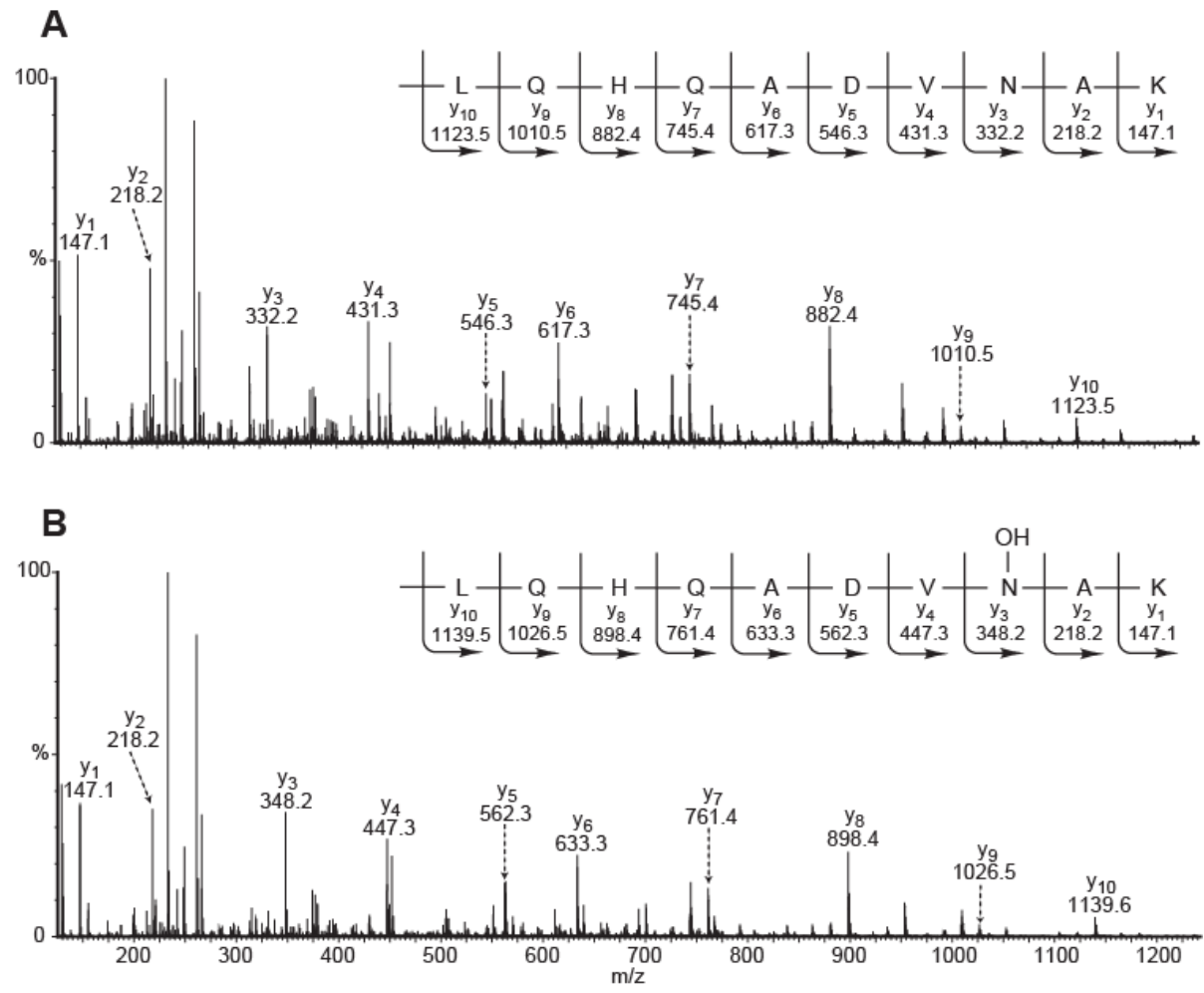


Figure S14

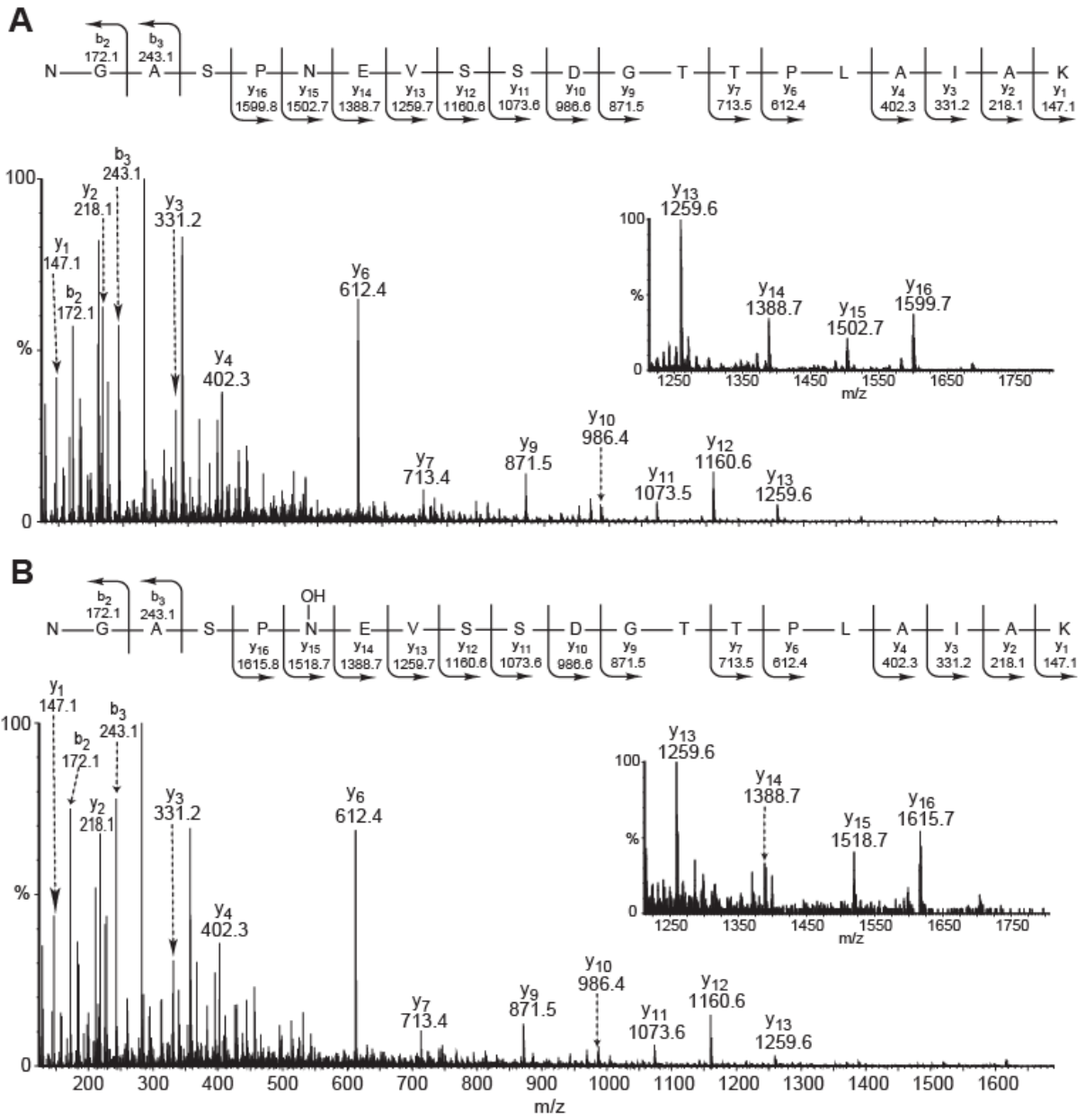


Figure S15

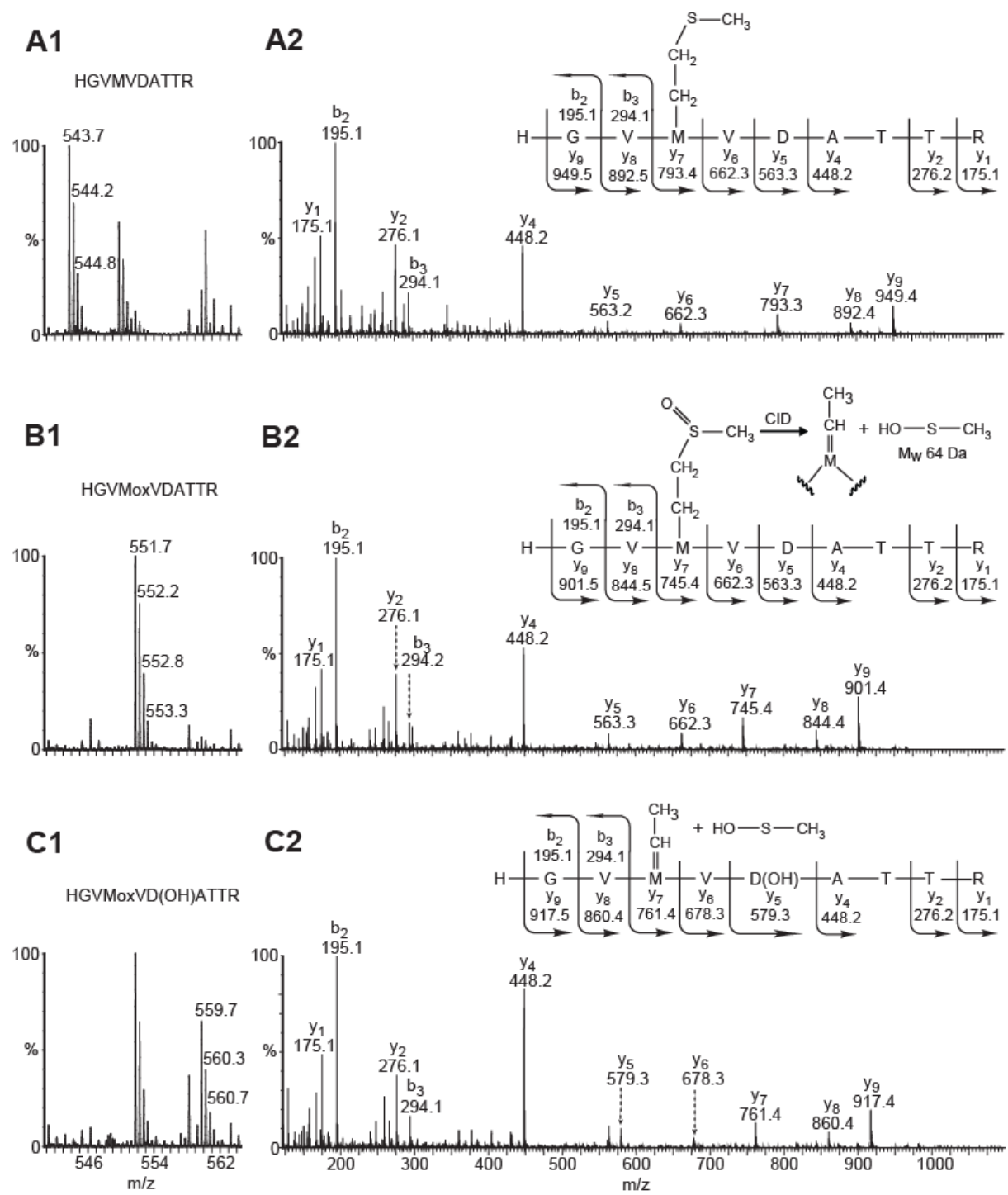


Figure S16

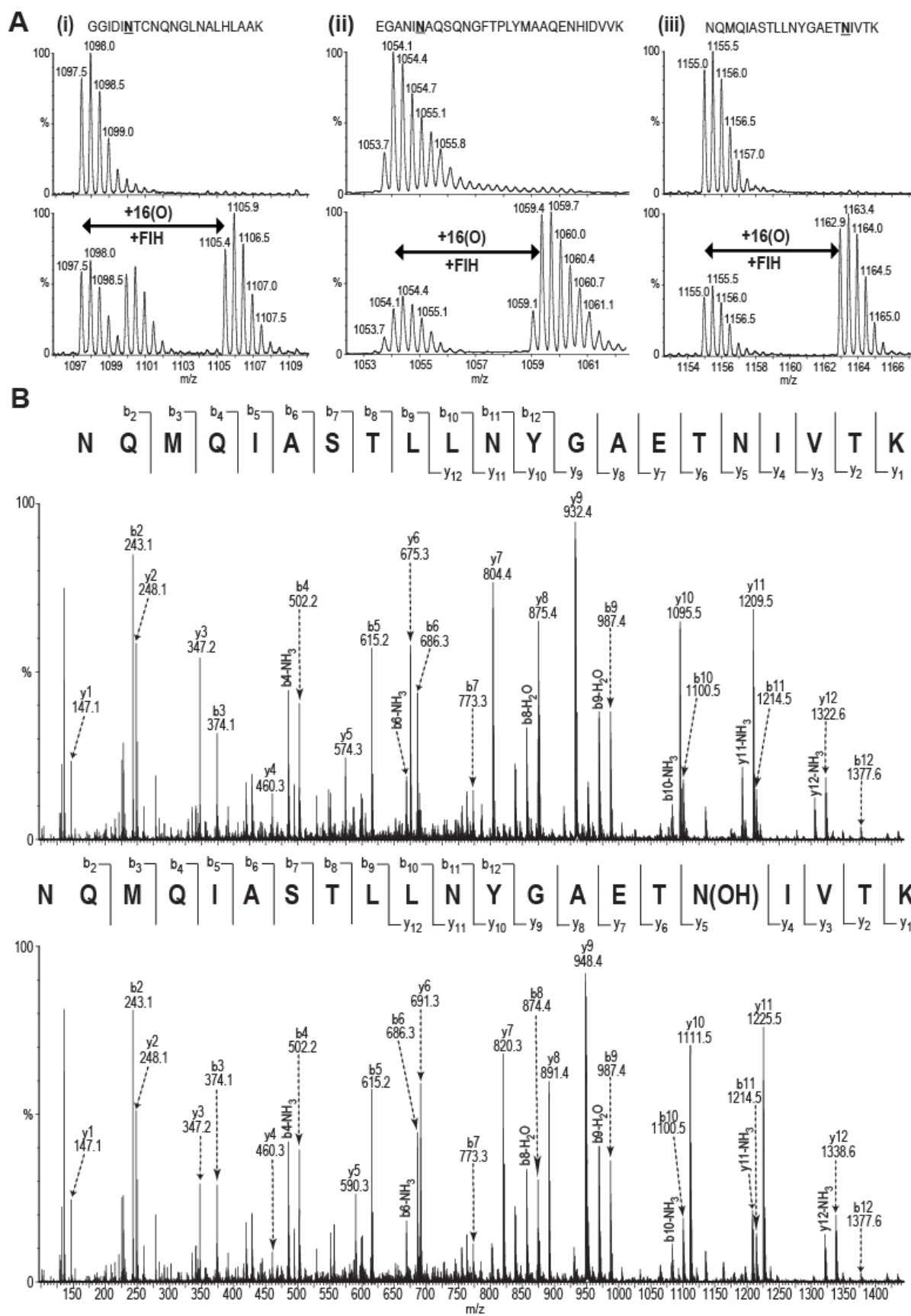


Figure S17

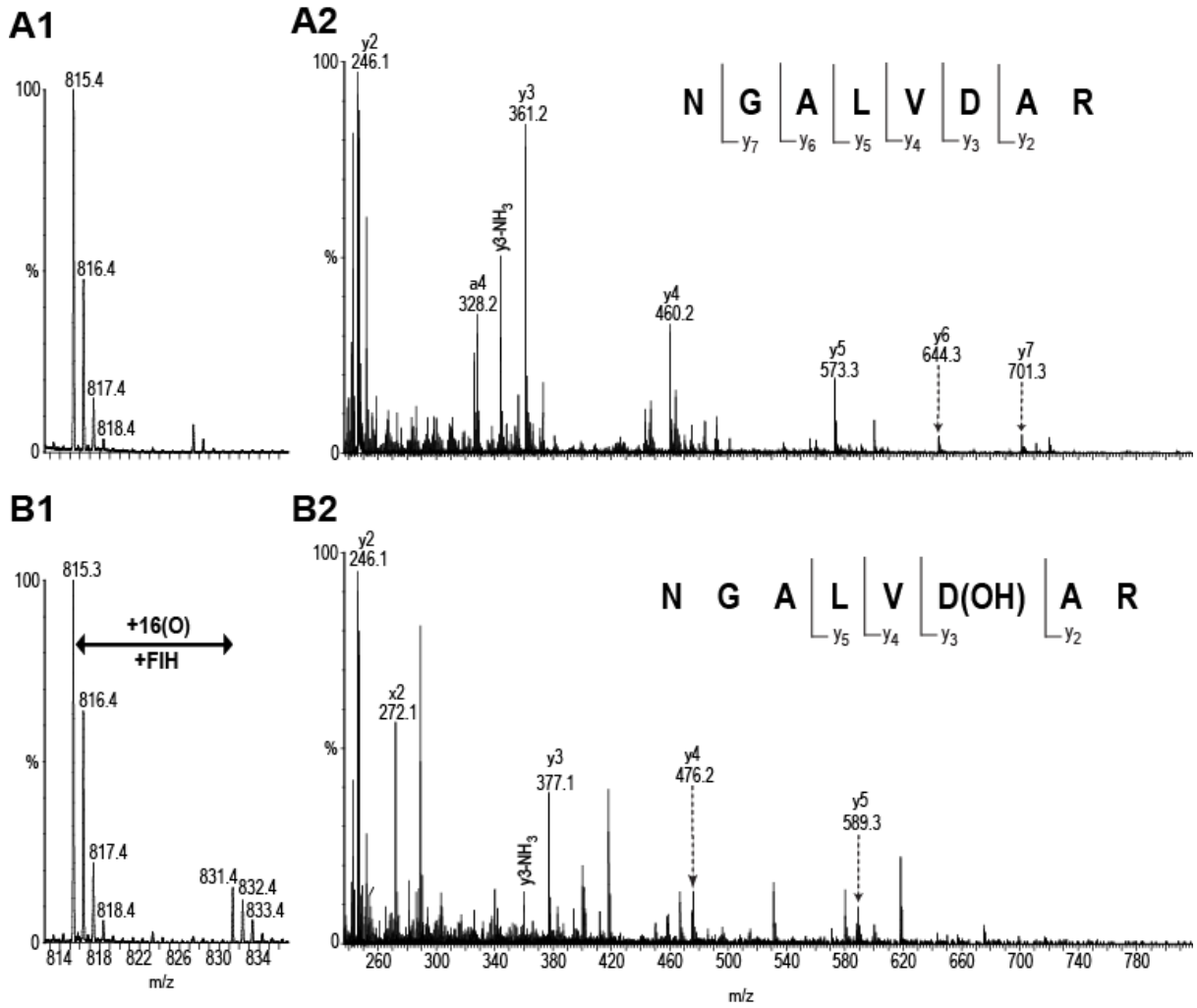


Figure S18

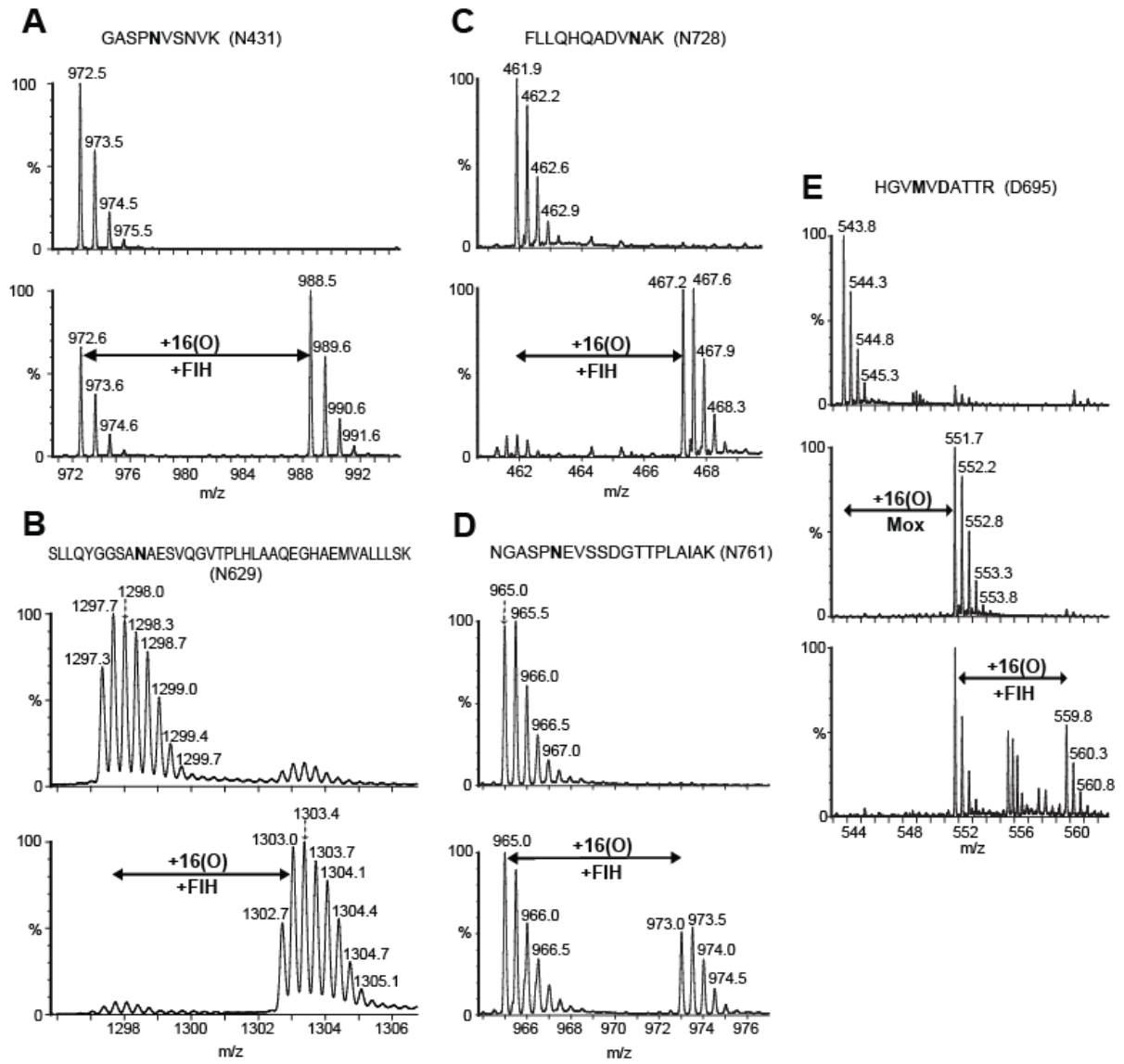


Figure S19

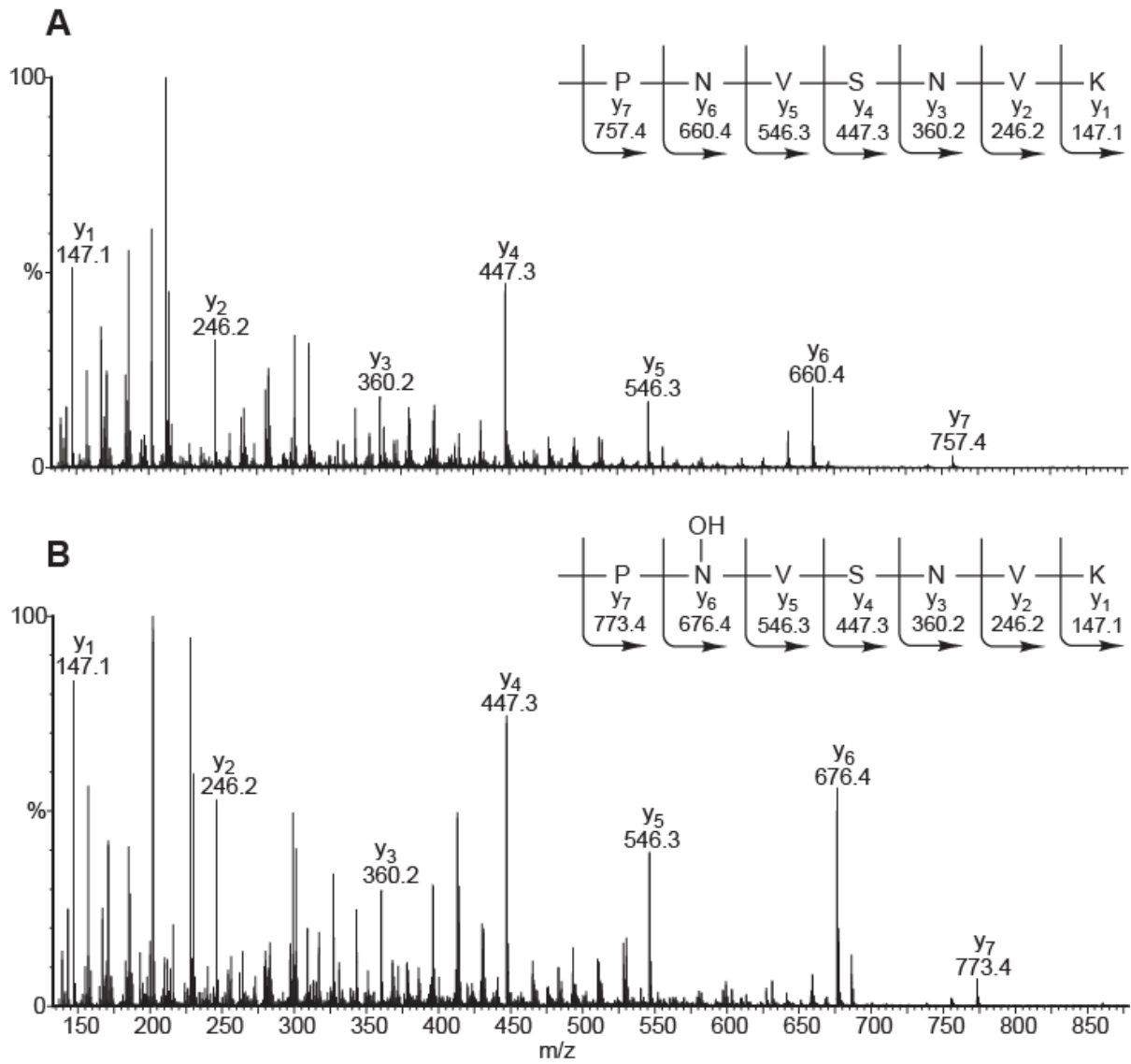
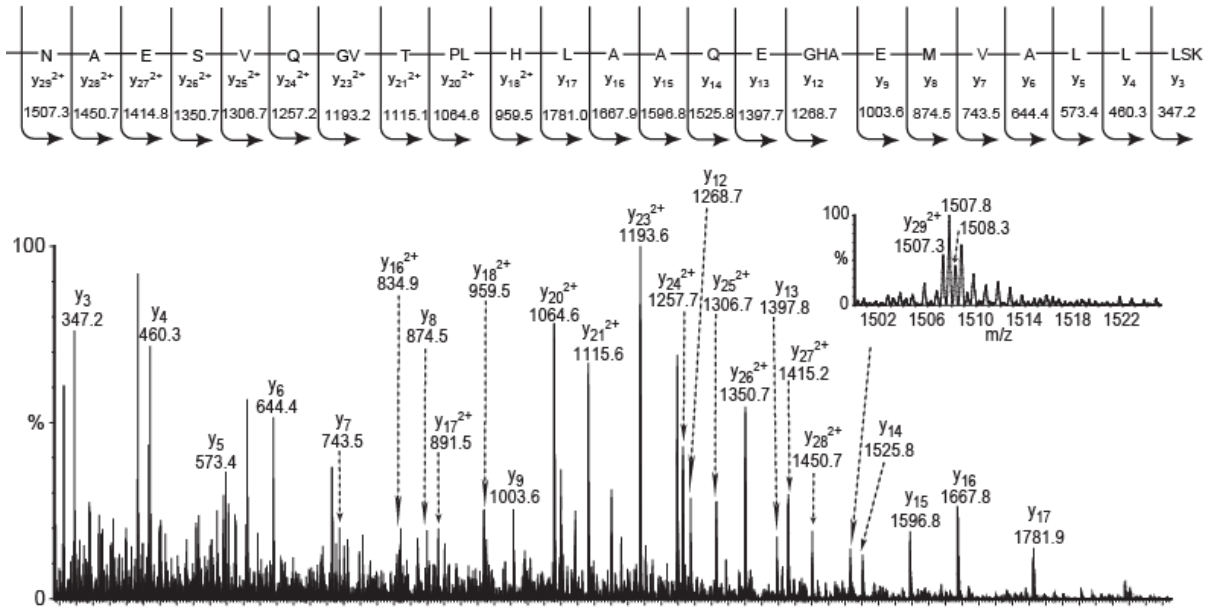


Figure S20

A



B

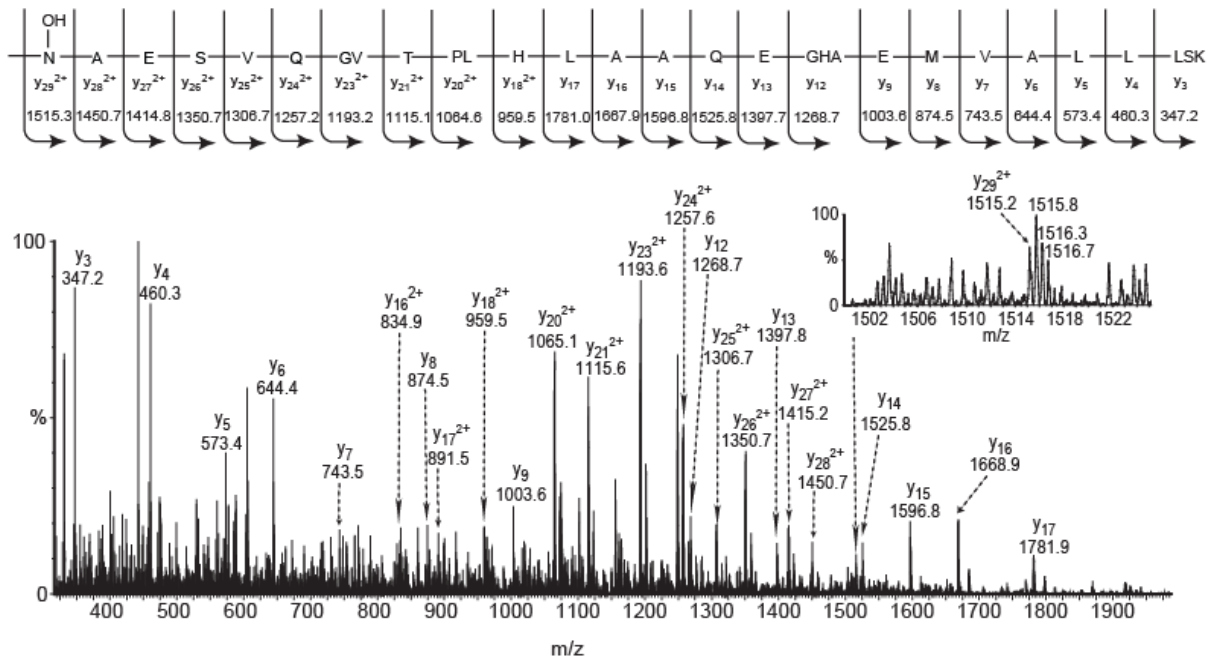


Figure S21

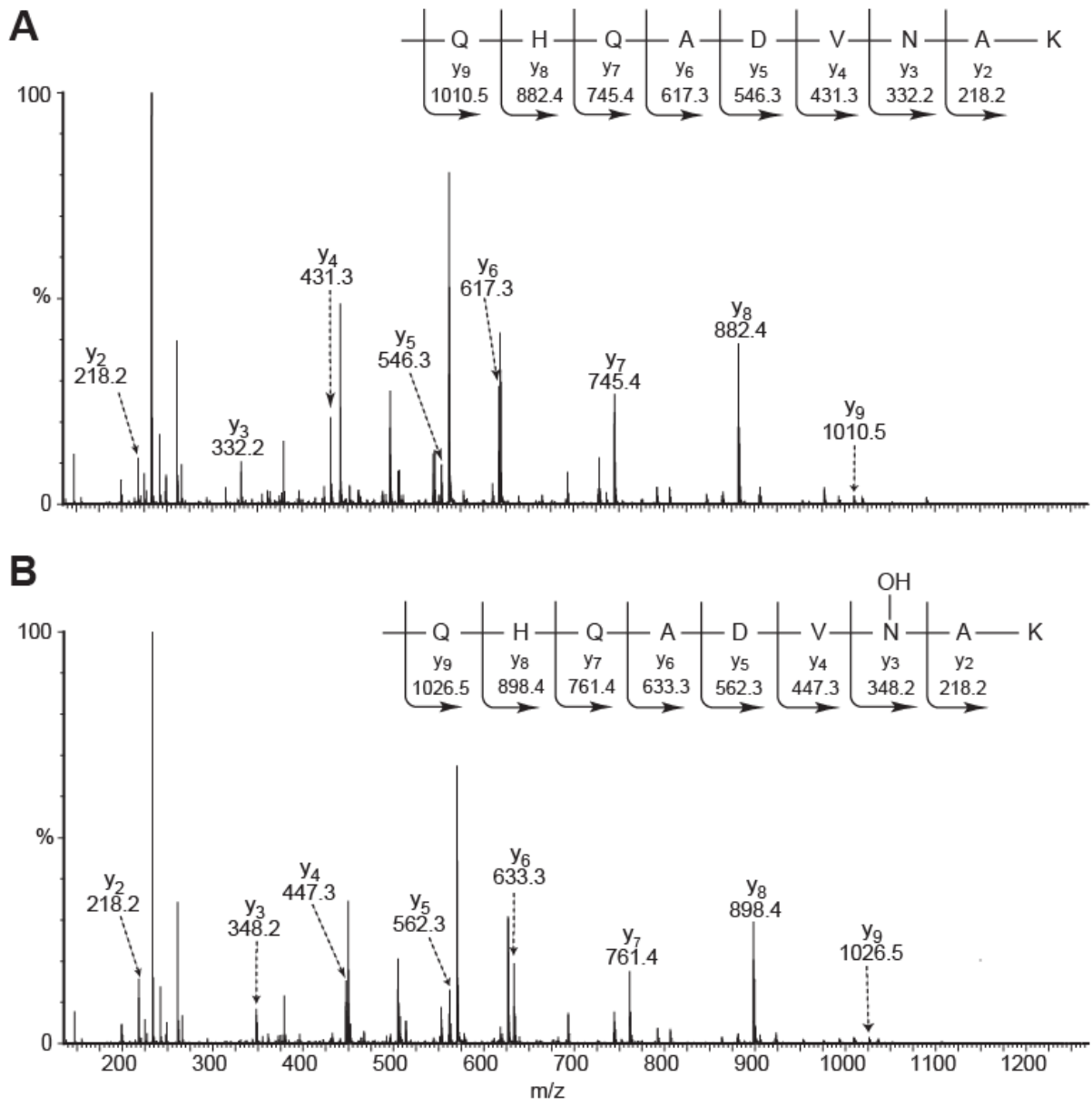
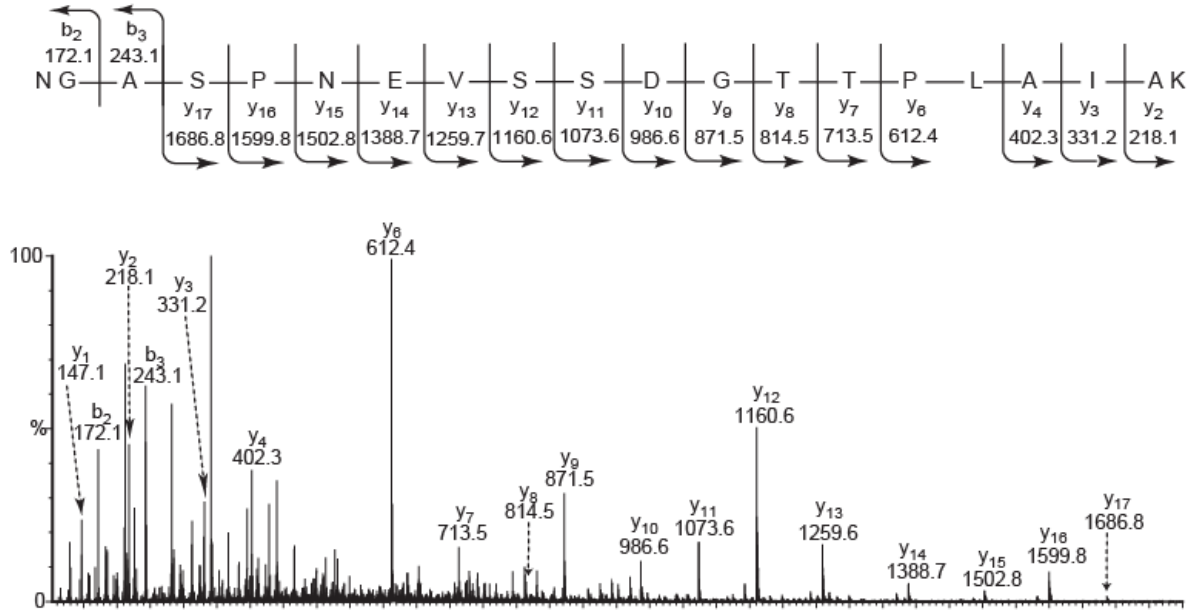


Figure S22

A



B

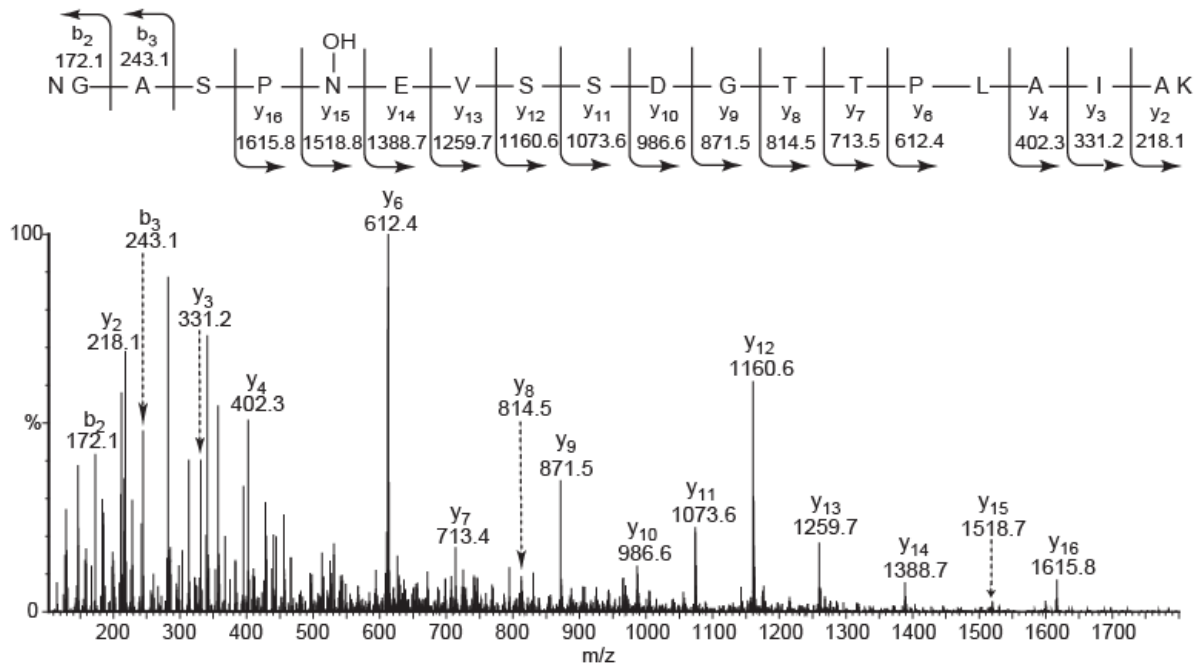


Figure S23

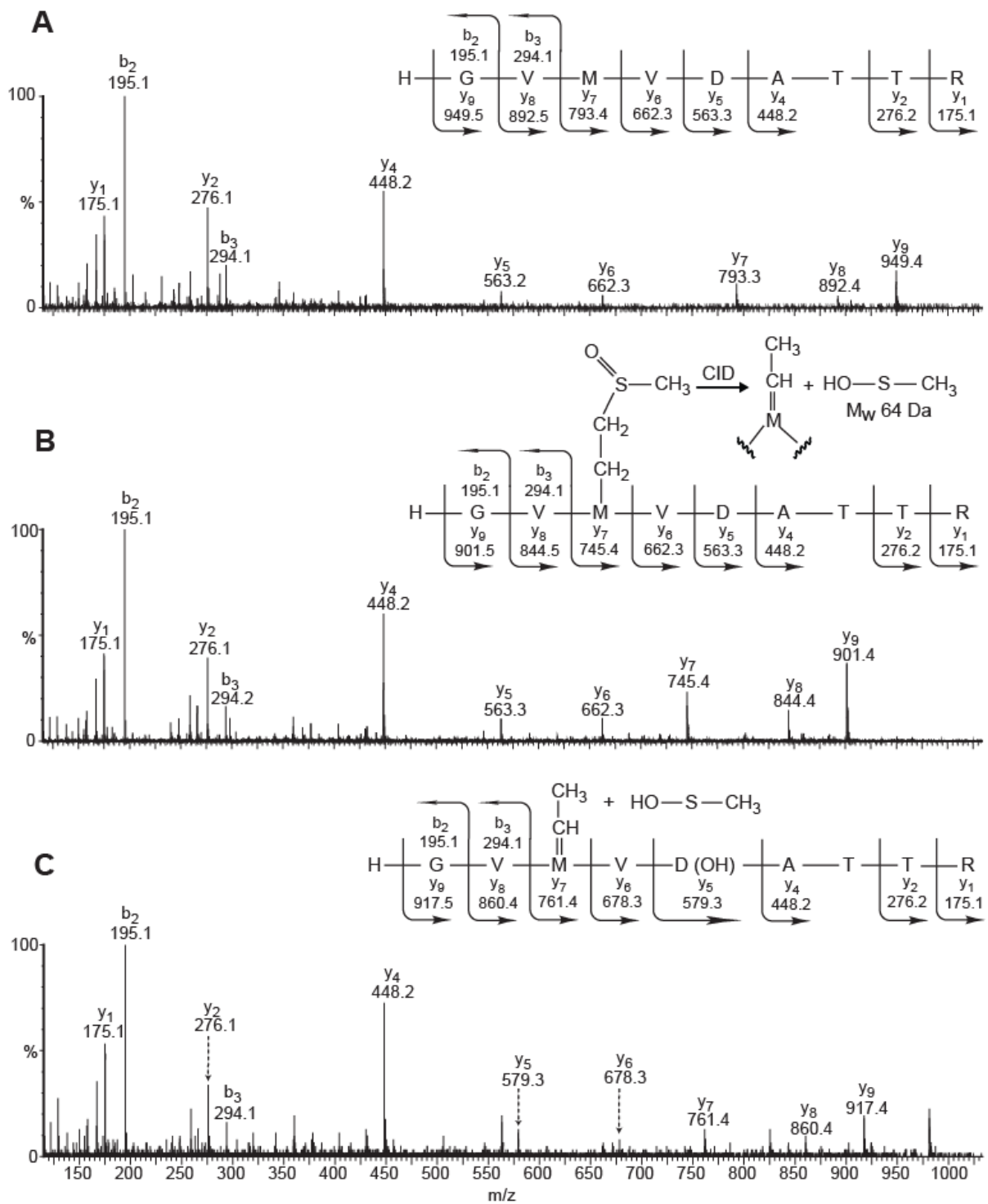


Figure S24

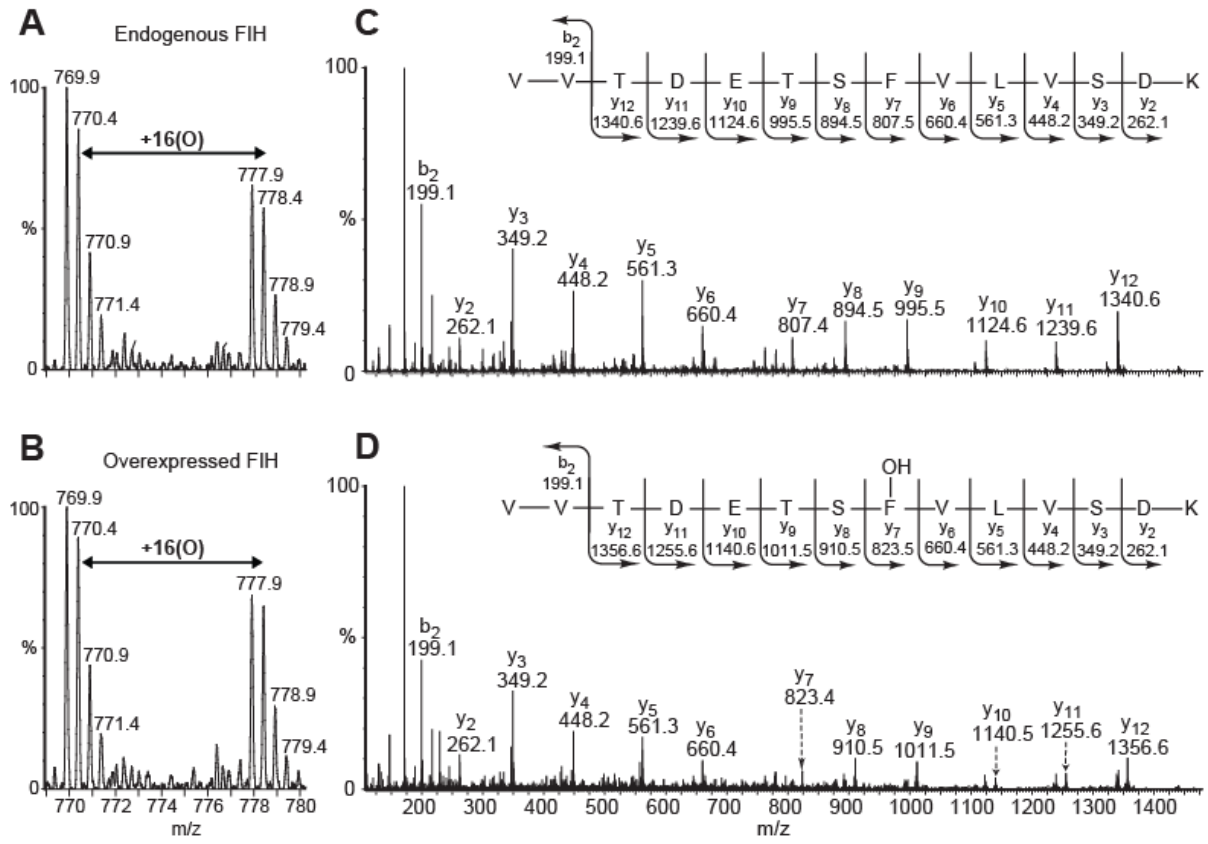


Figure S25

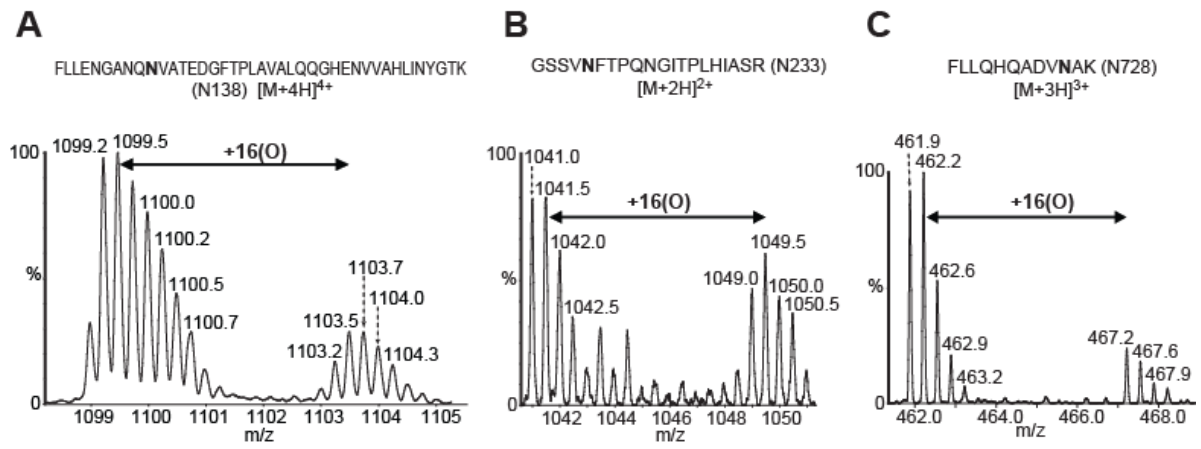


Figure S26

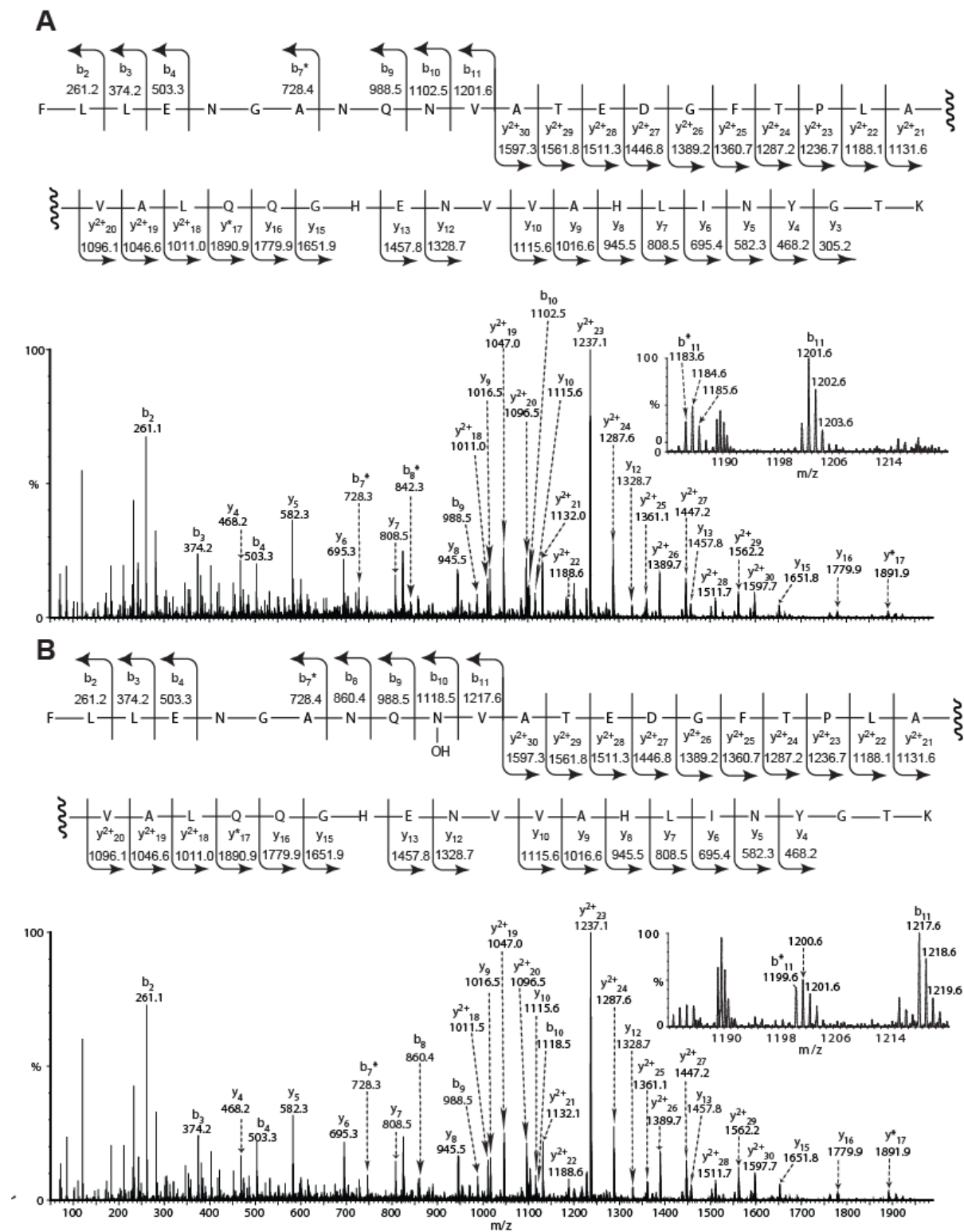


Figure S27

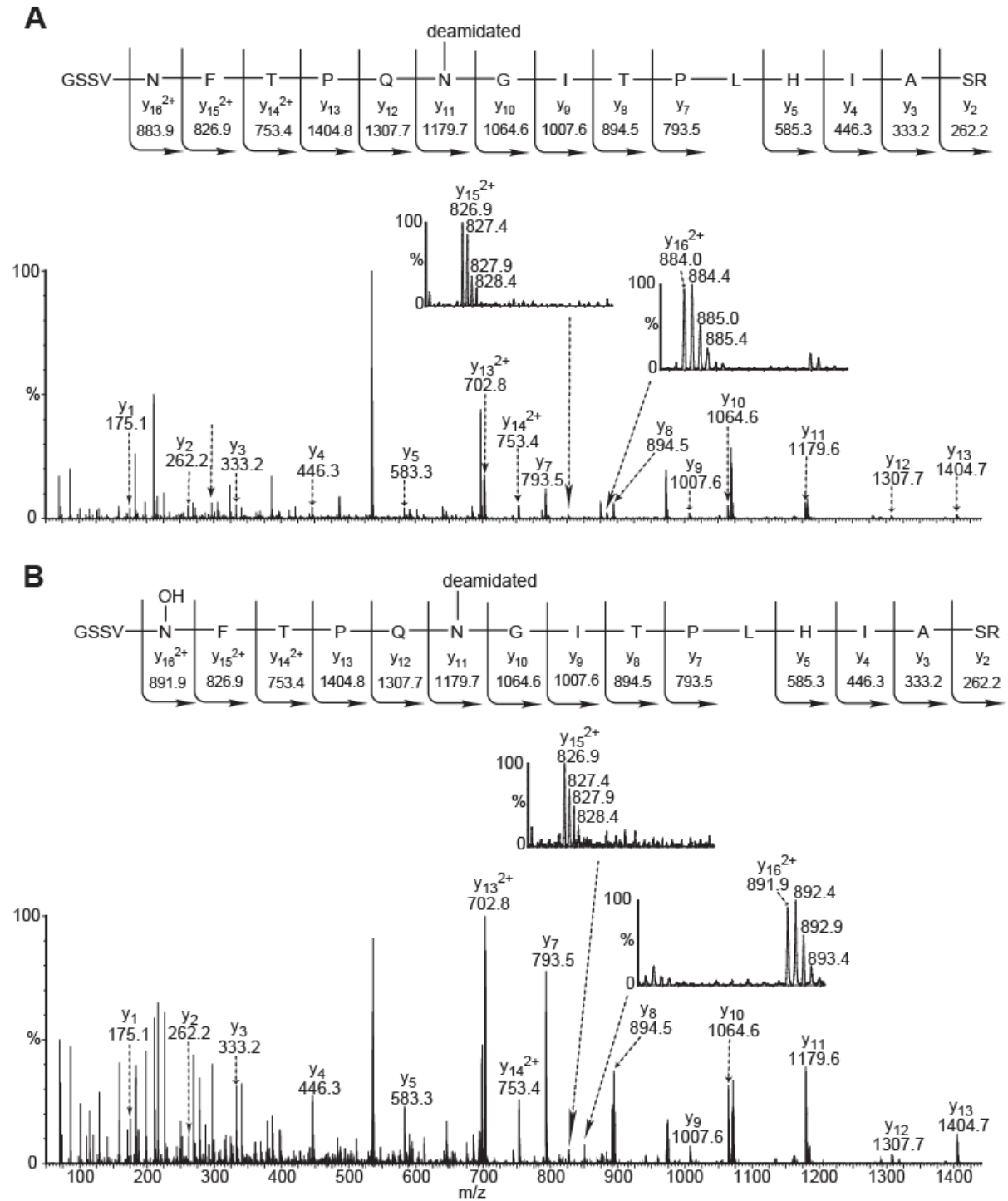


Figure S28

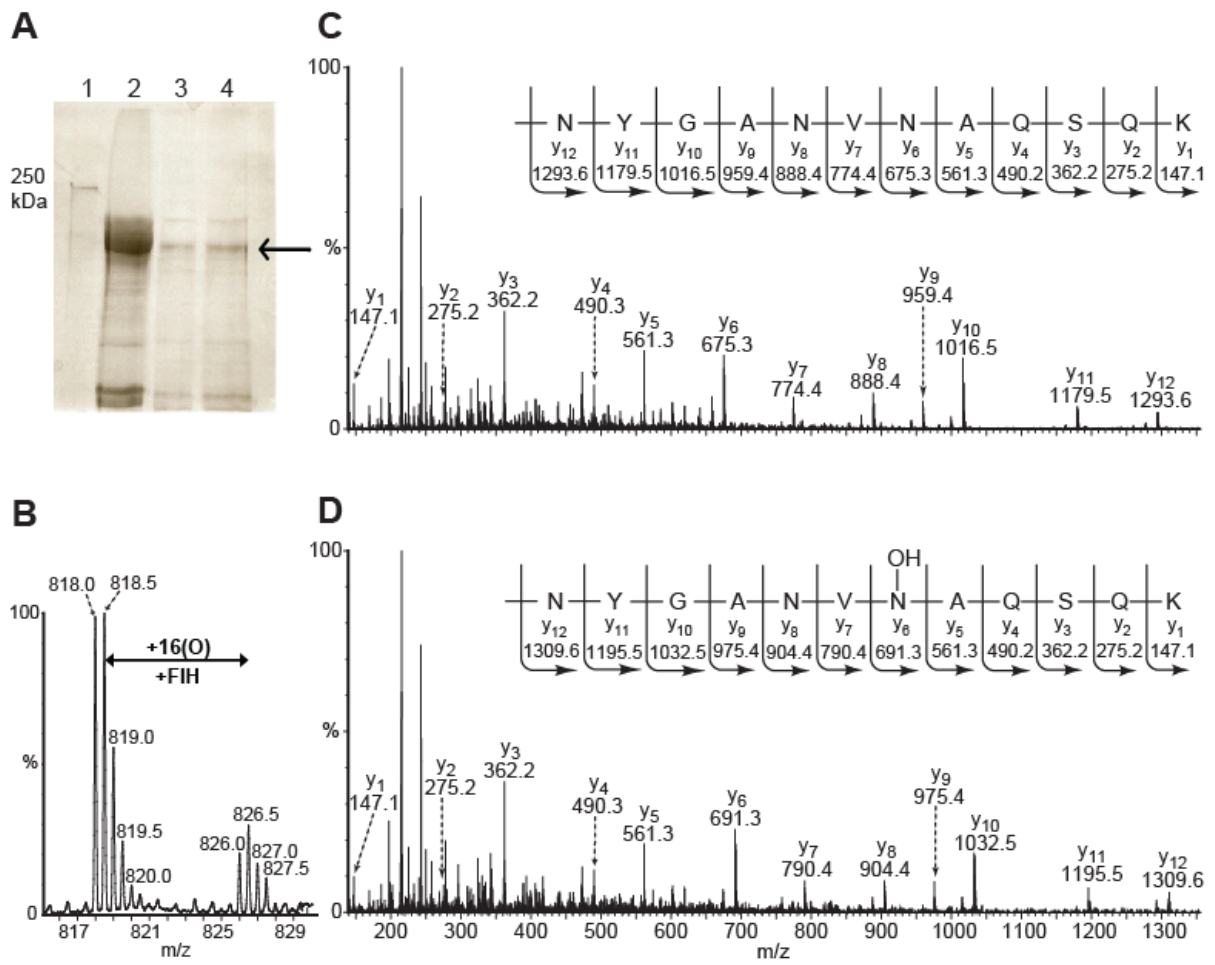


Figure S29

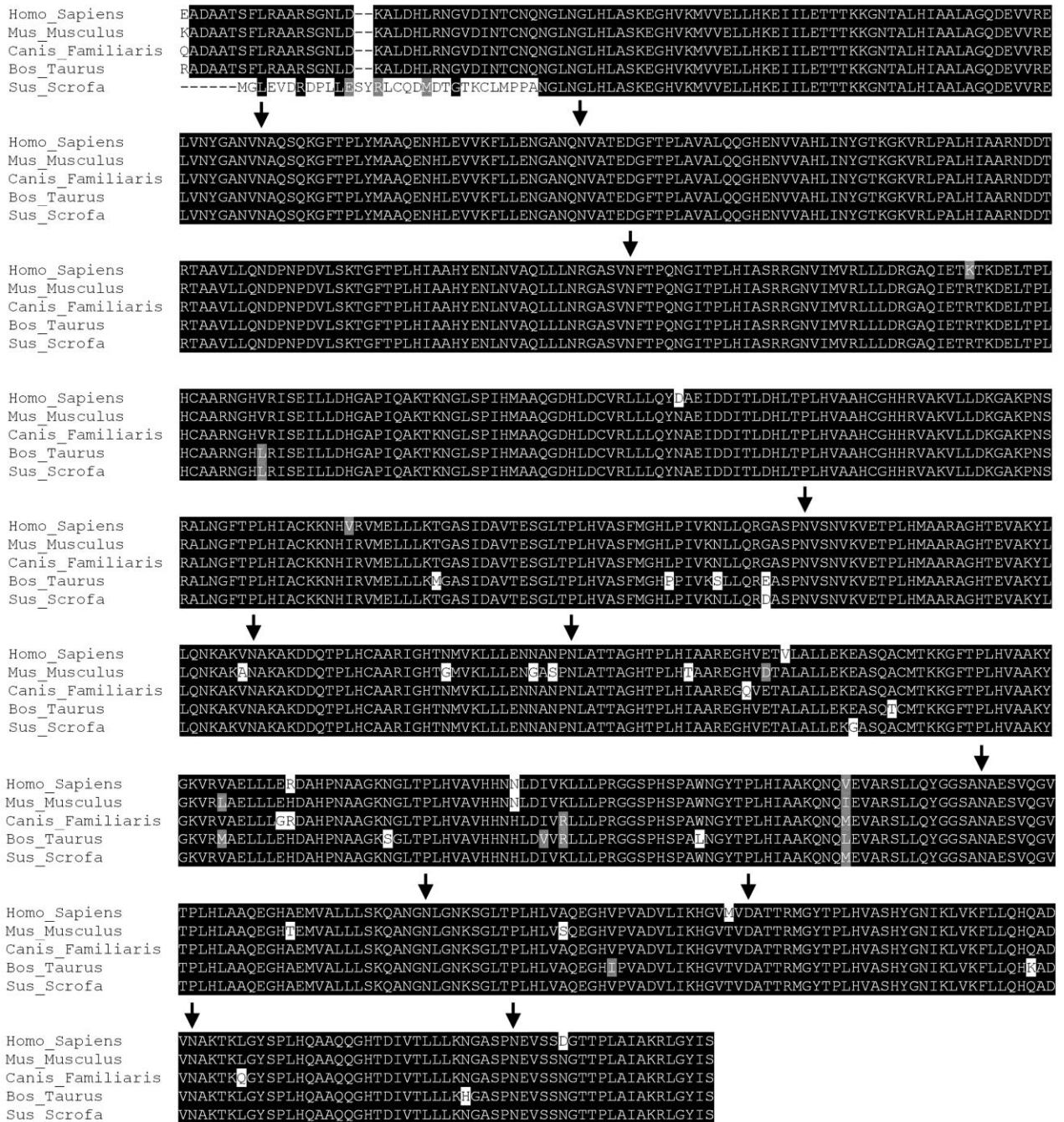


Figure S30

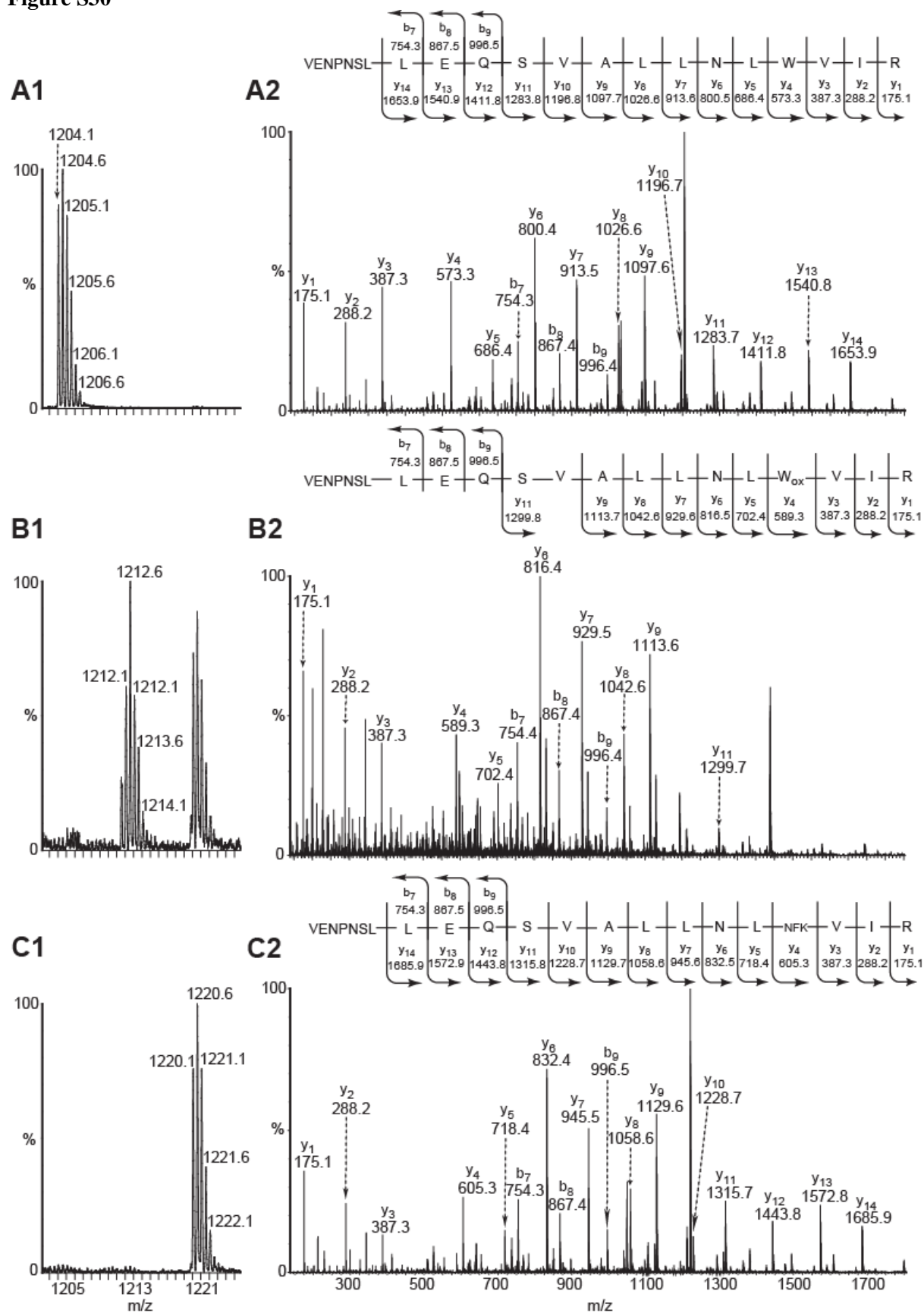


Figure S31

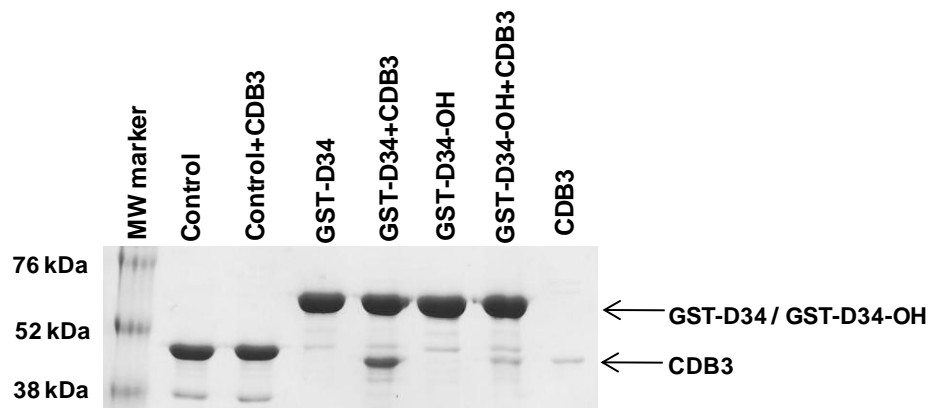


Figure S32

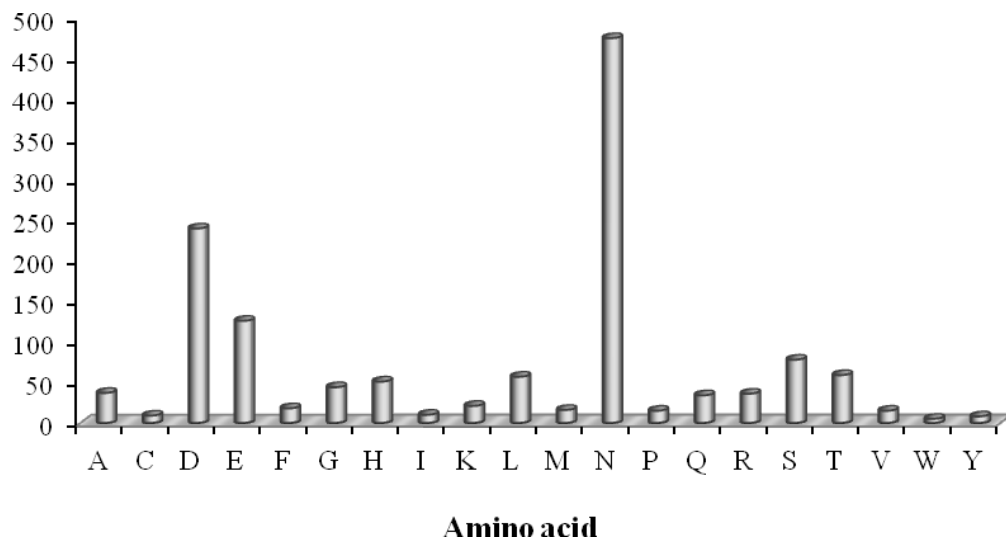


Figure S33

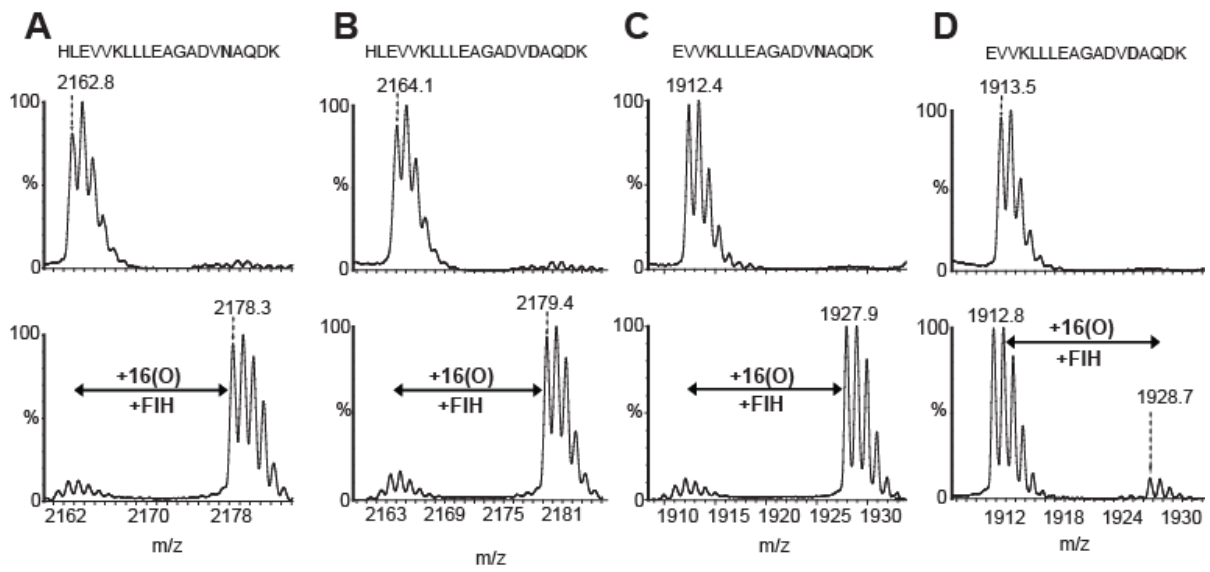


Figure S34

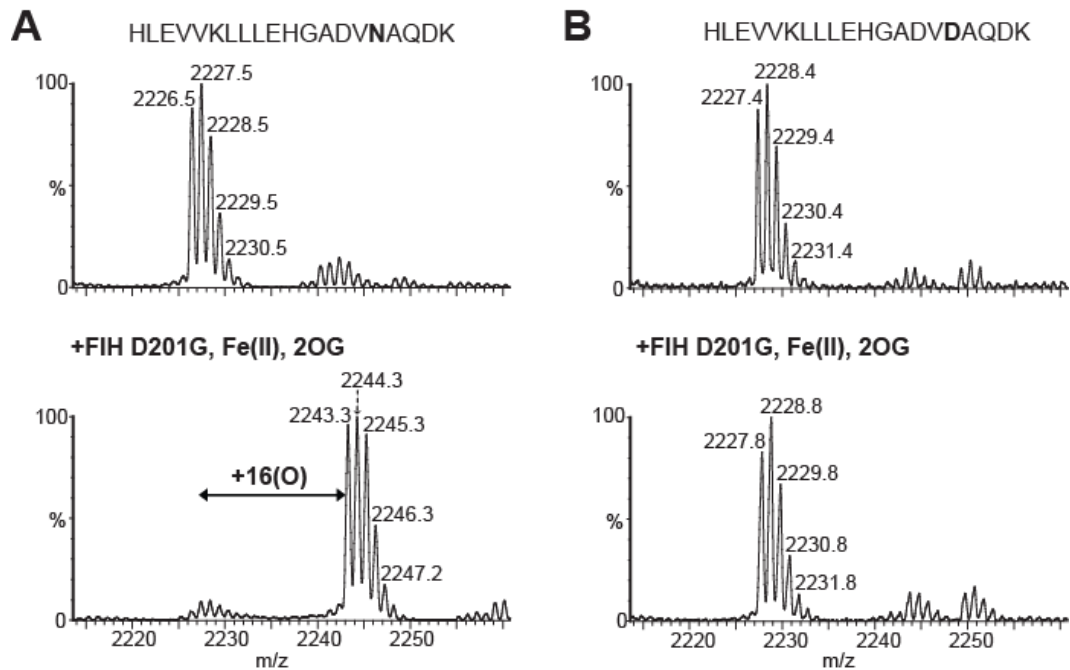


Figure S35

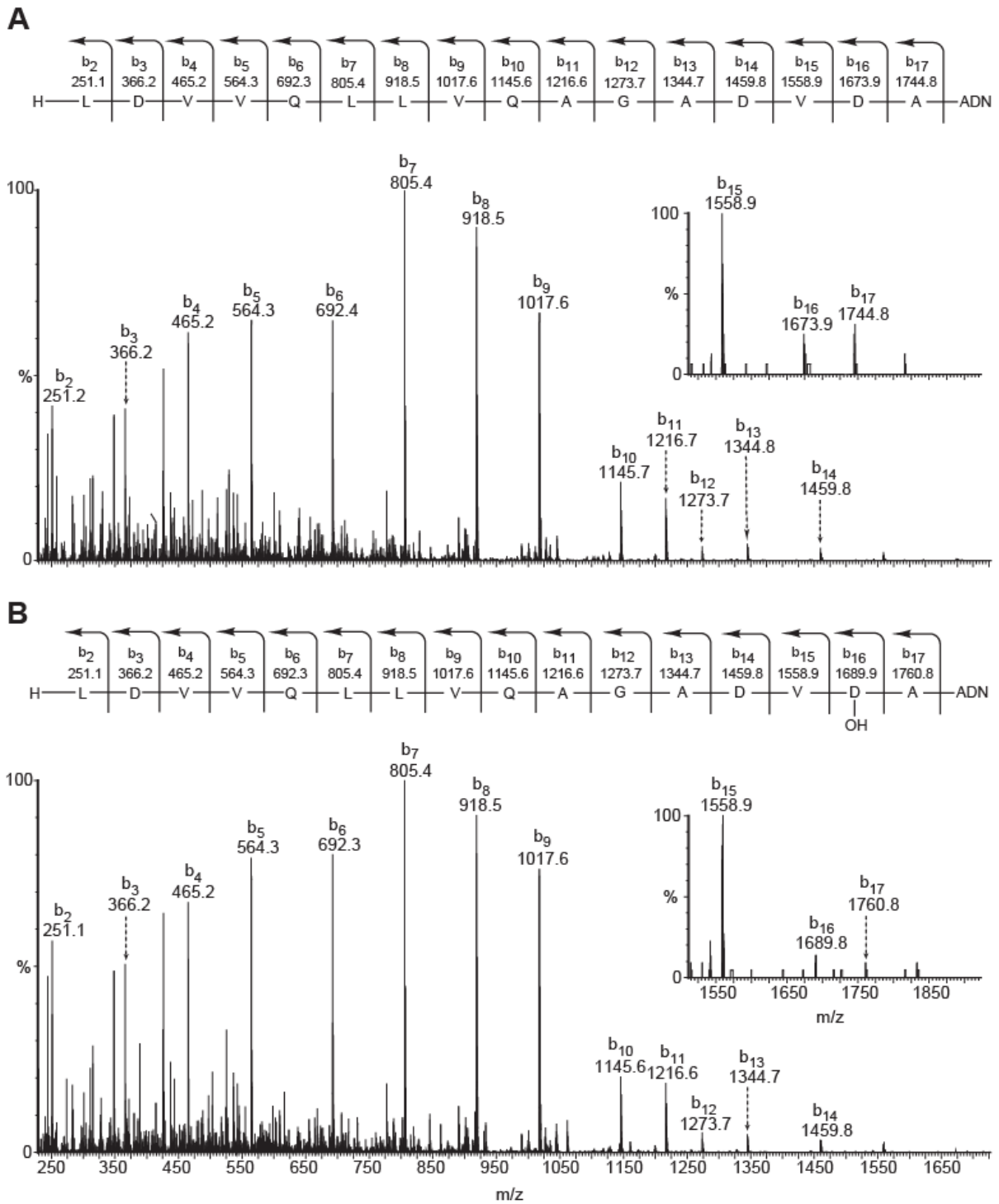


Figure S36

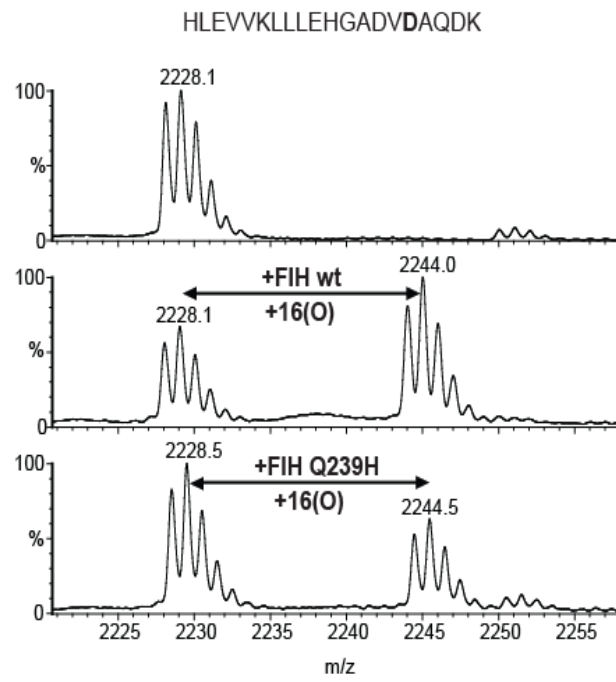


Figure S37

